Journal of Scientific Computing (2024) 98:70
https://doi.org/10.1007/s10915-024-02452-1

A Conservative Eulerian–Lagrangian Runge–Kutta Discontinuous Galerkin Method for Linear Hyperbolic System with Large Time Stepping

Xue Hong[1] · **Jing-Mei Qiu**[2]

Received: 18 May 2023 / Revised: 19 December 2023 / Accepted: 1 January 2024 /
Published online: 17 February 2024

Abstract

We propose an Eulerian–Lagrangian (EL) Runge–Kutta (RK) discontinuous Galerkin (DG) method for a linear hyperbolic system. The method is designed based on the ELDG method for transport problems (J Comput Phys 446:110,632, 2021), which tracks solutions along approximations to characteristics in the DG framework, allowing extra large time stepping sizes with stability with respect to the classical RKDG method. Considering each characteristic family, a straightforward application of ELDG for the hyperbolic system will be to transform to the characteristic variables, evolve them on associated characteristic-related space–time regions, and transform them back to the original variables. However, the conservation could not be guaranteed in a general setting. In this paper, we formulate a conservative semi-discrete ELDG method by decomposing each variable into two parts, each of them associated with a different characteristic family. As a result, four different quantities are evolved in EL fashion and recombined to update the solution. The fully discrete scheme is formulated by using method-of-lines RK methods, with intermediate RK solutions updated on the background mesh. Numerical results for 1D and 2D wave equations are presented to demonstrate the performance of the proposed ELDG method. These include the high order spatial and temporal accuracy, stability with extra large time stepping size, and conservative property.

Research of the first author is supported by the Centre Henri Lebesgue, program ANR-11-LABX-0020-0 and the Brittany council. Research of the second author is supported by NSF Grants NSF-DMS-1818924 and 2111253, Air Force Office of Scientific Research FA9550-22-1-0390 and Department of Energy DE-SC0023164.

✉ Jing-Mei Qiu
jingqiu@udel.edu

Xue Hong
xue.hong@inria.fr

[1] Inria Rennes (Mingus Team) and IRMAR UMR CNRS 6625, Université de Rennes, 35042 Rennes, France

[2] Department of Mathematical Sciences, University of Delaware, Newark, DE 19716, USA

Keywords Eulerian–Lagrangian · Discontinuous Galerkin · Characteristic method · Linear hyperbolic system · Conservative property

1 Introduction

In this paper, we propose an Eulerian–Lagrangian (EL) discontinuous Galerkin (DG) method for the first-order hyperbolic system in the form of

$$U_t + \sum_{j=1}^{d} (A_j(\mathbf{x}, t)U)_{x_j} = F(\mathbf{x}, t), \quad (\mathbf{x}, t) \in \mathbb{R}^d \times [0, T], \tag{1.1}$$

where d is the spatial dimension, $U : \mathbb{R}^d \times [0, T] \to \mathbb{R}^n$, and $A_j(\mathbf{x}, t) \in \mathbb{R}^{n\times d}$. Examples of such a system include the wave equations, Maxwell's equations, linearized shallow water equations. There are various versions of DG methods for solving hyperbolic systems, such as the Runge–Kutta DG methods [6] and the space–time DG methods [10, 18]. These methods belong to the class of Eulerian approach, thus suffer from the CFL condition. An alternative numerical approach is the characteristic method, which evolves a time-dependent solution by tracking characteristics. These class of methods are also known as semi-Lagrangian methods [2, 7, 9, 21] or Eulerian–Lagrangian methods [3, 4, 22]. The semi-Lagrangian method evolves a time-dependent solution by exactly tracking characteristics, while the Eulerian–Lagrangian method updates the solution via approximating characteristics by linear straight lines. For existing SL methods, some of them are developed by 1D versions using dimensional splitting [7, 9, 21], whereas others are purely 2D ones [2] to avoid the time-splitting error. In EL setting, an Eulerian Lagrangian Localized Adjoint Method (ELLAM) was developed in [4], by introducing an adjoint problem for each test function in the continuous finite element framework. Recently, the Eulerian–Lagrangian (EL) discontinuous Galerkin method(DG) [3, 22] and semi-Lagrangian (SL) DG [2] are being developed in the discontinuous Galerkin finite element framework with a similar introduction of adjoint problems for test functions. The ELDG method approximates characteristics by linear functions, which yields better stability with extra large upper bound for time stepping sizes compared with those from the classical Eulerian explicit RKDG method. The ELDG method is also closely related to the Arbitrary Lagrangian Eulerian (ALE) DG method [13, 14], which was introduced as a moving mesh DG method.

In this paper, we follow the scalar development of EL DG method, and propose a conservative EL DG method for hyperbolic systems (1.1). We start from 1D cases, for which we consider characteristic variables and the associated characteristic space–time regions. For hyperbolic systems, a straightforward application of EL DG to each characteristic family, on associated space–time regions can be done; yet the conservation could not be guaranteed in a general setting. In this work, we decompose each variable into two parts, each of which associated with different characteristic families. As a result, four different quantities are evolved in EL fashion and are recombined to update the solution. The fully discrete scheme is formulated by using method-of-lines RK methods, with intermediate RK solutions updated on the background mesh. For 2D hyperbolic systems, we use the dimensional splitting method, maintaining the simplicity, robustness and stability of ELDG methods for 1D cases. Note that, for 2D systems, characteristic Galerkin [19] or evolution Galerkin [1, 16, 17] methods have been proposed to take into account information propagated in all bicharacteristic directions.

This paper is organized as follows. In Sect. 2, we review the ELDG for one-dimensional (1D) linear transport problems. In Sect. 3, we develop the ELDG method for a first-order

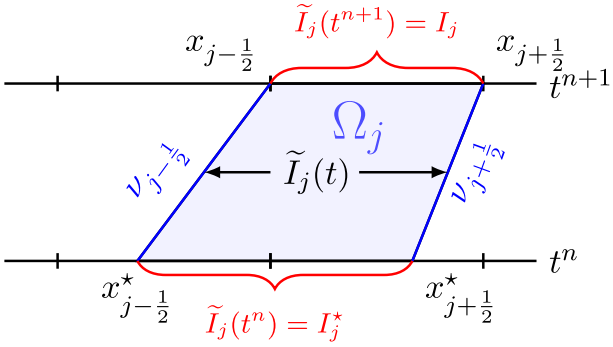

Fig. 1 Illustration for dynamic element $\widetilde{I}_j(t)$ of ELDG

hyperbolic system by decomposing and evolving each component into two parts, each of which associated with its characteristic family. 2D problems are handled by 1D algorithms with dimensional splitting. The conservation property is proved. In Sect. 4, performance of the proposed ELDG method is showcased through extensive numerical tests. Concluding remarks are made in Sect. 5.

2 Review of ELDG Formulation for 1D Linear Transport Problems [3]

To illustrate the key idea of the ELDG scheme, we start from a 1D linear transport equation in the following form

$$u_t + (a(x,t)u)_x = 0, \quad x \in [x_a, x_b]. \tag{2.1}$$

For simplicity, we assume periodic boundary conditions, and the velocity field $a(x,t)$ is a continuous function of space and time.

Discretization. The computational domain is partitioned as $x_a = x_{\frac{1}{2}} < x_{\frac{3}{2}} < \cdots < x_{N+\frac{1}{2}} = x_b$, called the background mesh. Let $I_j = [x_{j-\frac{1}{2}}, x_{j+\frac{1}{2}}]$ denote an element of length $\Delta x_j = x_{j+\frac{1}{2}} - x_{j-\frac{1}{2}}$ and define $\Delta x = \max_j \Delta x_j$. We define the finite dimensional approximation space, $V_h^k = \{v_h : v_h|_{I_j} \in P^k(I_j)\}$, where $P^k(I_j)$ denotes the set of polynomials of degree at most k on I_j. We let t^n be the n-th time level and $\Delta t = t^{n+1} - t^n$ to be the time-stepping size.

The key idea in the ELDG formulation is to design adjoint problems for test functions, taking advantage of information propagation along characteristics. The method is formulated on a space–time region $\Omega_j = \tilde{I}_j(t) \times [t^n, t^{n+1}]$ with

$$\tilde{I}_j(t) = \left[\tilde{x}_{j-\frac{1}{2}}(t), \tilde{x}_{j+\frac{1}{2}}(t)\right], \quad t \in \left[t^n, t^{n+1}\right],$$

being the dynamic interval with size $\Delta x_j(t) = \tilde{x}_{j+\frac{1}{2}}(t) - \tilde{x}_{j-\frac{1}{2}}(t)$, see Fig. 1. Here $\tilde{x}_{j\pm\frac{1}{2}}(t) = x_{j\pm\frac{1}{2}} + (t - t^{n+1})v_{j\pm\frac{1}{2}}$ are straight lines emanating from cell boundaries $x_{j\pm\frac{1}{2}}$ with slopes $v_{j\pm\frac{1}{2}} = a(x_{j\pm\frac{1}{2}}, t^{n+1})$ and $I_j^\star \doteq \tilde{I}_j(t^n) = [x^*_{j-\frac{1}{2}}, x^*_{j+\frac{1}{2}}]$ is the upstream cell of I_j at t^n.

A local adjoint problem of (2.1) for all test function is defined as:

$$\begin{cases} \psi_t + \alpha(x,t)\psi_x = 0, & (x,t) \in \Omega_j, \\ \psi(t = t^{n+1}) = \Psi(x). & \forall \Psi \in P^k(I_j). \end{cases} \tag{2.2}$$

Here $\alpha(x,t)$ is a bilinear function of (x,t) with

$$\begin{aligned}\alpha\left(x_{j-\frac{1}{2}},t^{n+1}\right)&=a\left(x_{j-\frac{1}{2}},t^{n+1}\right)\doteq v_{j-\frac{1}{2}},\\ \alpha\left(x_{j+\frac{1}{2}},t^{n+1}\right)&=a\left(x_{j+\frac{1}{2}},t^{n+1}\right)\doteq v_{j+\frac{1}{2}},\end{aligned}\tag{2.3}$$

and

$$\begin{aligned}\alpha(x,t)=&-v_{j-\frac{1}{2}}\frac{x-\tilde{x}_{j+\frac{1}{2}}(t)}{\Delta x_j(t)}+v_{j+\frac{1}{2}}\frac{x-\tilde{x}_{j-\frac{1}{2}}(t)}{\Delta x_j(t)}\\ &\in P^1(\tilde{I}_j(t)),\quad \forall t\in[t^n,t^{n+1}].\end{aligned}\tag{2.4}$$

The ELDG [3] scheme can be formulated by $\int_{\tilde{I}_j(t)}(2.2)\cdot u+(2.1)\cdot\psi$

$$\frac{d}{dt}\int_{\tilde{I}_j(t)}(u\psi)dx=-\left(\hat{F}\psi\right)\Big|_{\tilde{x}_{j+\frac{1}{2}}(t)}+\left(\hat{F}\psi\right)\Big|_{\tilde{x}_{j-\frac{1}{2}}(t)}+\int_{\tilde{I}_j(t)}F\psi_x dx.\tag{2.5}$$

where $F(u)\doteq(a-\alpha)u$ and $\hat{F}$ is the Lax–Friedrichs flux. A method-of-lines RK discretization can be used for high order temporal accuracy [3].

3 The ELDG Algorithm for Hyperbolic System

In this section, we design the ELDG algorithm for a 1D hyperbolic system, in a similar spirit as the 1D scalar case, but tracking information along different characteristics families.

3.1 1D Hyperbolic System

We consider the hyperbolic system

$$U_t+(A(x)U)_x=F(x,t),\tag{3.1}$$

where $U=\left[u^1,u^2\right]^T$ is a column vector, A is a 2 by 2 matrix, and F is a 2 by 1 vector. We use the following notations for the eigen-decomposition of $A(x)$:

- eigenvalue: $\lambda^{(1)}(x),\quad \lambda^{(2)}(x)$.
- $A(x)=R(x)\Lambda R^{-1}(x)$, where $\Lambda(x)=diag(\lambda^{(1)}(x),\lambda^{(2)}(x))$,

$$R(x)\doteq\left[r^{(1)}(x)\mid r^{(2)}(x)\right]=\begin{bmatrix}r_{11}(x)&r_{12}(x)\\ r_{21}(x)&r_{22}(x)\end{bmatrix}\tag{3.2}$$

contains the right column eigenvectors $r^{(1)},\ r^{(2)}$, and

$$R^{-1}(x)\doteq\begin{bmatrix}l^{(1)^T}(x)\\ l^{(2)^T}(x)\end{bmatrix}=\begin{bmatrix}l_{11}(x)&l_{12}(x)\\ l_{21}(x)&l_{22}(x)\end{bmatrix}\tag{3.3}$$

contains the left row eigenvectors $l^{(1)^T},\ l^{(2)^T}$. From $R\cdot R^{-1}=I$, we have

$$\begin{aligned}(r_{11}(x)l^{(1)^T}(x)+r_{12}(x)l^{(2)^T}(x))U(x)&=u^1,\\ (r_{21}(x)l^{(1)^T}(x)+r_{22}(x)l^{(2)^T}(x))U(x)&=u^2.\end{aligned}\tag{3.4}$$

In the following, we propose a conservative ELDG scheme for the system (3.1) by the procedure below.

(1) Partitions of space–time regions $\Omega_j^{(1)}$ and $\Omega_j^{(2)}$. According to the first and second characteristic families, we partition the computational domain as two sets of space–time regions $\Omega_j^{(1)}$ and $\Omega_j^{(2)}$ respectively. Here $\Omega_j^{(1)} = \tilde{I}_j^{(1)}(t) \times [t^n, t^{n+1}]$ is related to the first characteristic family. $\tilde{I}_j^{(1)}(t) = [\tilde{x}^{(1)}_{j-\frac{1}{2}}(t), \tilde{x}^{(1)}_{j+\frac{1}{2}}(t)]$ is the dynamic interval emanating from cell boundaries $x_{j\pm\frac{1}{2}}$ with slopes $\nu^{(1)}_{j\pm\frac{1}{2}}$ approximating the first characteristic velocity, see Fig. 2(left). In general, we choose $\nu^{(1)}_{j\pm\frac{1}{2}} = \lambda^{(1)}(x_{j\pm\frac{1}{2}})$. $I_j^{\star,(1)} \doteq \tilde{I}_j^{(1)}(t^n)$ is the upstream cell of I_j from the first characteristic family at t^n. Similar definition can be made to $\Omega_j^{(2)}$, $\tilde{I}_j^{(2)}(t)$ and $I_j^{\star,(2)}$ for the second characteristic family. See Fig. 2(right) for illustration of $\Omega_j^{(2)}$.

(2) Adjoint Problems. We consider an adjoint problem for the first characteristic family on $\Omega_j^{(1)}$:

$$\begin{cases} (\psi^{(1)})_t + \alpha^{(1)}(\psi^{(1)})_x = 0, & t \in [t^n, t^{n+1}], \\ (\psi^{(1)})(t = t^{n+1}) = \Psi^{(1)}(x), \end{cases} \tag{3.5}$$

where

$$\alpha^{(1)}(x,t) = -\nu^{(1)}_{j-\frac{1}{2}} \frac{x - \tilde{x}^{(1)}_{j+\frac{1}{2}}(t)}{\Delta x_j^{(1)}(t)} + \nu^{(1)}_{j+\frac{1}{2}} \frac{x - \tilde{x}^{(1)}_{j-\frac{1}{2}}(t)}{\Delta x_j^{(1)}(t)} \in P^1(\tilde{I}_j^{(1)}(t)). \tag{3.6}$$

Similarly on $\Omega_j^{(2)}$:

$$\begin{cases} (\psi^{(2)})_t + \alpha^{(2)}(\psi^{(2)})_x = 0, & t \in [t^n, t^{n+1}], \\ (\psi^{(2)})(t = t^{n+1}) = \Psi^{(2)}(x), \end{cases} \tag{3.7}$$

where

$$\alpha^{(2)}(x,t) = -\nu^{(2)}_{j-\frac{1}{2}} \frac{x - \tilde{x}^{(2)}_{j+\frac{1}{2}}(t)}{\Delta x_j^{(2)}(t)} + \nu^{(2)}_{j+\frac{1}{2}} \frac{x - \tilde{x}^{(2)}_{j-\frac{1}{2}}(t)}{\Delta x_j^{(2)}(t)} \in P^1(\tilde{I}_j^{(2)}(t)). \tag{3.8}$$

The adjoint problems provide finite dimensional time-dependent test function space, please see more details in Appendix B.

(3) Formulation of a conservative semi-discrete ELDG scheme. For linear hyperbolic system, a straightforward generalization of ELDG is to transform the original variable to the characteristic variables by a localized eigen-decomposition, that are consistent between two characteristic families. In particular, we take the vector product of $r_{11}(x){l^{(1)}}^T(x)$ from left with (3.1) and obtain a scalar equation

$$r_{11}(x){l^{(1)}}^T(x)(U_t + (A(x)U)_x) = r_{11}(x){l^{(1)}}^T(x)F(x,t). \tag{3.9}$$

Multiply $\psi^{(1)}$ to the equation above, we get

$$r_{11}(x){l^{(1)}}^T(x)(U_t + (A(x)U)_x)\psi^{(1)} = r_{11}(x){l^{(1)}}^T(x)F(x,t)\psi^{(1)}. \tag{3.10}$$

Meanwhile, multiply (3.5) from the left by $r_{11}(x){l^{(1)}}^T(x)U$, we have

$$r_{11}(x){l^{(1)}}^T(x)U(\psi^{(1)})_t + r_{11}(x){l^{(1)}}^T(x)U\alpha^{(1)}(\psi^{(1)})_x = 0. \tag{3.11}$$

Sum Eqs. (3.10) and (3.11), and integrate over the space–time interval $\Omega_j^{(1)}$,

$$\begin{aligned}
&\int_{\Omega_j^{(1)}} \Big(r_{11}(x){l^{(1)}}^T(x)U_t\psi^{(1)} + r_{11}(x){l^{(1)}}^T(x)U(\psi^{(1)})_t \\
&\quad + r_{11}(x){l^{(1)}}^T(x)(A(x)U)_x\psi^{(1)} \Big)\, dxdt \\
&\quad + \int_{\Omega_j^{(1)}} r_{11}(x){l^{(1)}}^T(x)U\alpha^{(1)}(\psi^{(1)})_x dxdt \\
&= \int_{\Omega_j^{(1)}} r_{11}(x){l^{(1)}}^T(x)F(x,t)\psi^{(1)} dxdt.
\end{aligned} \tag{3.12}$$

A further manipulation on the left hand side (L.H.S.) of (3.12) gives

$$\begin{aligned}
&\int_{\Omega_j^{(1)}} \Big((r_{11}(x){l^{(1)}}^T(x)U\psi^{(1)})_t + r_{11}(x){l^{(1)}}^T(x)(A(x)U)_x\psi^{(1)} \\
&\quad + r_{11}(x){l^{(1)}}^T(x)U\alpha^{(1)}(\psi^{(1)})_x \Big)\, dxdt \\
&= \int_{\Omega_j^{(1)}} \Big((r_{11}(x){l^{(1)}}^T(x)U\psi^{(1)})_t + (r_{11}(x){l^{(1)}}^T(x)A(x)U\psi^{(1)})_x \\
&\quad - (r_{11}(x){l^{(1)}}^T(x))_x A(x)U\psi^{(1)} \Big)\, dxdt \\
&\quad - \int_{\Omega_j^{(1)}} \Big(r_{11}(x){l^{(1)}}^T(x)A(x)U(\psi^{(1)})_x - r_{11}(x){l^{(1)}}^T(x)U\alpha^{(1)}(\psi^{(1)})_x \Big)\, dxdt \\
&= \int_{t^n}^{t^{n+1}} \Bigg(\frac{d}{dt} \int_{\tilde{I}_j^{(1)}(t)} (r_{11}(x){l^{(1)}}^T U\psi^{(1)})dx \\
&\quad + [r_{11}(x){l^{(1)}}^T A(x)U\psi^{(1)} - \nu^{(1)} r_{11}(x){l^{(1)}}^T U\psi^{(1)}]\Big|_{j-\frac{1}{2}}^{j+\frac{1}{2}} \Bigg)\, dt \\
&\quad - \int_{t^n}^{t^{n+1}} \int_{\tilde{I}_j^{(1)}(t)} \Big((r_{11}(x){l^{(1)}}^T(x))_x A(x)U\psi^{(1)} \\
&\quad + r_{11}(x){l^{(1)}}^T(x)(A(x)U - \alpha^{(1)}U)\psi_x^{(1)} \Big)\, dxdt.
\end{aligned} \tag{3.13}$$

Letting $f^{11}(U) = r_{11}{l^{(1)}}^T(AU - \alpha^{(1)}U)$, the time differential form of (3.12) with (3.13) gives

$$\begin{aligned}
&\frac{d}{dt} \int_{\tilde{I}_j^{(1)}(t)} (r_{11}(x){l^{(1)}}^T(x)U\psi^{(1)})dx + \Big(f^{11}\psi^{(1)} \Big)\Big|_{\tilde{x}_{j+\frac{1}{2}}^{(1)}(t)} \\
&\quad - \Big(f^{11}\psi^{(1)} \Big)\Big|_{\tilde{x}_{j-\frac{1}{2}}^{(1)}(t)} - \int_{\tilde{I}_j^{(1)}(t)} f^{11}\psi_x^{(1)} dx \\
&\quad - \int_{\tilde{I}_j^{(1)}(t)} (r_{11}(x){l^{(1)}}^T(x))_x A(x)U\psi^{(1)} dx
\end{aligned}$$

$$= \int_{\tilde{I}_j^{(1)}(t)} r_{11}(x) l^{(1)^T}(x) F(x,t) \psi^{(1)} dx. \tag{3.14}$$

Similarly, we have an equation related to $\lambda^{(2)}$

$$\begin{aligned} &\frac{d}{dt}\int_{\tilde{I}_j^{(1)}(t)} (r_{12}(x) l^{(2)^T}(x) U \psi^{(2)}) dx + \left(f^{12}\psi^{(2)}\right)\Big|_{\tilde{x}^{(2)}_{j+\frac{1}{2}}(t)} \\ &\quad - \left(f^{12}\psi^{(2)}\right)\Big|_{\tilde{x}^{(2)}_{j-\frac{1}{2}}(t)} - \int_{\tilde{I}_j^{(2)}(t)} f^{12}\psi_x^{(2)} dx \\ &\quad - \int_{\tilde{I}_j^{(2)}(t)} (r_{12}(x) l^{(2)^T}(x))_x A(x) U \psi^{(2)} dx \\ &= \int_{\tilde{I}_j^{(2)}(t)} r_{12}(x) l^{(2)^T}(x) F(x,t) \psi^{(2)} dx, \end{aligned} \tag{3.15}$$

where $f^{12}(U) = r_{12} l^{(2)^T}(AU - \alpha^{(2)} U)$. Then, we can update u^1 by (3.4) together with (3.14), (3.15), taking $\Psi^{(1)}(x) = \Psi(x)$ in (3.5) and $\Psi^{(2)}(x) = \Psi(x)$ in (3.7):

$$\begin{aligned} \int_{I_j} u^{1,n+1}\Psi(x) dx &\overset{(3.4)}{=} \int_{I_j} r_{11} l^{(1)^T} U^{n+1} \Psi(x) dx \\ &+ \int_{I_j} r_{12} l^{(2)^T} U^{n+1} \Psi(x) dx \\ &= \int_{I_j^{*,(1)}} r_{11} l^{(1)^T} U^n \psi^{(1)} dx - \int_{t^n}^{t^{n+1}} \left(f^{11}\psi^{(1)}\right)\Big|_{\tilde{x}^{(1)}_{j+\frac{1}{2}}(t)} + \left(f^{11}\psi^{(1)}\right)\Big|_{\tilde{x}^{(1)}_{j-\frac{1}{2}}(t)} dt \\ &+ \int_{t^n}^{t^{n+1}} \int_{\tilde{I}_j^{(1)}(t)} r_{11}(x) l^{(1)^T}(x) F(x,t) \psi^{(1)} \\ &+ (r_{11}(x) l^{(1)^T}(x))_x A(x) U \psi^{(1)} + f^{11}\psi_x^{(1)} dx dt \\ &+ \int_{I_j^{*,(2)}} r_{12} l^{(2)^T} U^n \psi^{(2)} dx \\ &- \int_{t^n}^{t^{n+1}} \left(f^{12}\psi^{(2)}\right)\Big|_{\tilde{x}^{(2)}_{j+\frac{1}{2}}(t)} + \left(f^{12}\psi^{(2)}\right)\Big|_{\tilde{x}^{(2)}_{j-\frac{1}{2}}(t)} dt \\ &+ \int_{t^n}^{t^{n+1}} \int_{\tilde{I}_j^{(2)}(t)} r_{12}(x) l^{(2)^T}(x) F(x,t) \psi^{(2)} \\ &+ (r_{12}(x) l^{(2)^T}(x))_x A(x) U \psi^{(2)} + f^{12}\psi_x^{(2)} dx dt. \end{aligned} \tag{3.16}$$

The ELDG discretization of Eq. (3.16) is to find $u_h^1(x,t) \in P^k(I_j(t))$, so that

$$\begin{aligned} &\int_{I_j} u_h^1(x, t^{n+1})\Psi(x) dx \\ &= \int_{I_j^{*,(1)}} r_{11} l^{(1)^T} U_h^n \psi^{(1)} dx + \int_{t^n}^{t^{n+1}} L_{11}(U_h(t), t, \tilde{I}_j^{(1)}(t)) dt \end{aligned}$$

$$+\int_{I_j^{*,(2)}} r_{12} l^{(2)^T} U_h^n \psi^{(2)} dx + \int_{t^n}^{t^{n+1}} L_{12}(U_h(t), t, \tilde{I}_j^{(2)}(t)) dt, \tag{3.17}$$

for $\psi^{(1)}(x,t)$ satisfying the adjoint problem (3.5) with $\forall \Psi(x) = \psi(x, t^{n+1}) \in P^k(I_j)$. Here

$$\begin{aligned}
&L_{11}(U_h(t), t, \tilde{I}_j^{(1)}(t)) \\
&= -\widehat{f^{11}_{j+\frac{1}{2}}} \psi^{(1),-}_{j+\frac{1}{2}} + \widehat{f^{11}_{j-\frac{1}{2}}} \psi^{(1),+}_{j-\frac{1}{2}} + \int_{\tilde{I}_j^{(1)}(t)} f^{11} \psi_x^{(1)}(x,t) dx \\
&\quad + \int_{\tilde{I}_j^{(1)}(t)} (r_{11} l^{(1)^T})_x A U_h \psi^{(1)}(x,t) + r_{11} l^{(1)^T} F \psi^{(1)}(x,t) dx, \\
&L_{12}(U_h(t), t, \tilde{I}_j^{(2)}(t)) \\
&= -\widehat{f^{12}_{j+\frac{1}{2}}} \psi^{(2),-}_{j+\frac{1}{2}} + \widehat{f^{12}_{j-\frac{1}{2}}} \psi^{(2),+}_{j-\frac{1}{2}} + \int_{\tilde{I}_j^{(2)}(t)} f^{12} \psi_x^{(2)}(x,t) dx \\
&\quad + \int_{\tilde{I}_j^{(2)}(t)} (r_{12} l^{(2)^T})_x A U_h \psi^{(2)}(x,t) + r_{12} l^{(2)^T} F \psi^{(2)}(x,t) dx,
\end{aligned} \tag{3.18}$$

where $\psi^{(1),\pm}_{j\pm\frac{1}{2}} = \psi^{(1)}(x^{(1),\pm}_{j\pm\frac{1}{2}}(t), t)$ and $\widehat{f^{11}}$ at a cell boundary can be taken as a monotone flux, e.g. the Lax–Friedrichs flux

$$\widehat{f^{11}_{j+\frac{1}{2}}}(U) = r_{11}(x_{j+\frac{1}{2}}) l^{(1)^T}(x_{j+\frac{1}{2}}) \left(A \cdot \widehat{U - \nu^{(1)}_{j+\frac{1}{2}} U}\right)_{j+\frac{1}{2}}.$$

$\psi^{(2),\pm}_{j\pm\frac{1}{2}} = \psi^{(2)}(x^{(2),\pm}_{j\pm\frac{1}{2}}(t), t)$ and $\widehat{f^{12}}$ can be similarly defined at a cell boundary. We can similarly obtain the ELDG scheme for u_h^2.

(4) Fully discrete ELDG scheme with method-of-lines RK schemes. To update (3.17) from U_h^n to U_h^{n+1}, we first apply the forward Euler time discretization to get 1st order accuracy, then we generalize the scheme to general RK methods. There are two main steps involved here.

In order to describe the implementation procedure of the fully discrete ELDG scheme, we define the L^2 projection.

Definition 3.1 (L^2 projection) Let $u \in L^2(\Omega)$, $M = \{I_j\}_{j=1}^N$ and $\tilde{M} = \{\tilde{I}_j\}_{j=1}^N$ be two different meshes of the whole computational domain Ω. We have function spaces $V_h^k = \{u : u|_{I_j} \in P^k(I_j), \forall j\}$ and $\tilde{V}_h^k = \{\tilde{u} : \tilde{u}|_{\tilde{I}_j} \in P^k(\tilde{I}_j), \forall j\}$ corresponding to meshes M and $\tilde{M}$. The L^2 projection of $u_M \in V_h^k$ onto space $\tilde{V}_h^k$ can be defined as, find $\tilde{u}_{\tilde{M}} \in \tilde{V}_h^k$, s.t.

$$\int_{\tilde{I}_j} \tilde{u}_{\tilde{M}}(x) \varphi(x) dx = \int_{\tilde{I}_j} u_M(x) \varphi(x) dx, \ \forall \varphi \in \tilde{V}_h^k. \tag{3.19}$$

We denote $\tilde{u}_{\tilde{M}}(x) = Proj[u_M(x); M, \tilde{M}]$. The evaluation of the right hand side of (3.19) can be done in a subinterval-by-subinterval fashion. The implementation details can be found in [12].

Then, we propose a fully discrete ELRKDG scheme with procedure as described:

(a) **Obtain the initial condition on upstream meshes $\tilde{I}_j^{(1)}(t^n)$ and $\tilde{I}_j^{(2)}(t^n)$** of (3.17) by $U_h^{n,(1)} = Proj[U_h^n; I_j, \tilde{I}_j^{(1)}(t^n)]$ and $U_h^{n,(2)}(t^n) = Proj[U_h^n; I_j, \tilde{I}_j^{(2)}(t^n)]$, which are the L^2 projections of solutions from the background mesh to the upstream mesh.

(b) **Update** (3.17) **from** U_h^n to U_h^{n+1}, **component-by-component.**

(a) Get the mesh information of the dynamic element $\tilde{I}_j^{(1)}(t^{(l)})$, $l = 0, \ldots, s$ on RK stages by $\tilde{x}_{j\pm\frac{1}{2}}^{(1)}(t) = x_{j\pm\frac{1}{2}} + (t - t^{n+1})v_{j\pm\frac{1}{2}}^{(1)}$. Here $s = 1$ for forward-Euler method and $s = 2$ for Heun's method (SSPRK2), see the blue domain in Fig. 2 and for explicit midpoint RK2 with intermediate stage in Fig. 3.

(b1) For forward-Euler method, compute

$$
\begin{aligned}
&\int_{I_j} u_h^{1,n+1}\Psi(x)dx \\
&= \int_{I_j^{*,(1)}} r_{11}l^{(1)^T}U_h^n\psi^{(1),n}dx + \Delta t L_{11}(U_h^n, t^n, \tilde{I}_j^{(1)}(t^n)) \\
&\quad + \int_{I_j^{*,(2)}} r_{12}l^{(2)^T}U_h^n\psi^{(2),n}dx + \Delta t L_{12}(U_h^n, t^n, \tilde{I}_j^{(2)}(t^n)) \\
&= \int_{I_j^{*,(1)}} r_{11}l^{(1)^T}U_h^n\psi^{(1),n}dx \\
&\quad + \Delta t\left(-\widehat{f^{11}_{j+\frac{1}{2}}}(U_h^{n,(1)})\psi^{(1),n,-}_{j+\frac{1}{2}} + \widehat{f^{11}_{j-\frac{1}{2}}}(U_h^{n,(1)})\psi^{(1),n,+}_{j-\frac{1}{2}}\right. \\
&\quad + \int_{I_j^{*,(1)}} f^{11}(U_h^{n,(1)})\psi_x^{(1)}(x,t^n)dx + \int_{I_j^{*,(1)}} (r_{11}l^{(1)^T})_x AU_h^n\psi^{(1)}(x,t^n)dx \\
&\quad \left. + \int_{I_j^{*,(1)}} r_{11}l^{(1)^T}F(x,t^n)\psi^{(1)}(x,t^n)dx\right) \\
&\quad + \int_{I_j^{*,(2)}} r_{12}l^{(2)^T}U_h^n\psi^{(2),n}dx \\
&\quad + \Delta t\left(-\widehat{f^{12}_{j+\frac{1}{2}}}(U_h^{n,(2)})\psi^{(2),n,-}_{j+\frac{1}{2}} + \widehat{f^{12}_{j-\frac{1}{2}}}(U_h^{n,(2)})\psi^{(2),n,+}_{j-\frac{1}{2}}\right. \\
&\quad + \int_{I_j^{*,(2)}} f^{12}(U_h^{n,(2)})\psi_x^{(2)}(x,t^n)dx + \int_{I_j^{*,(2)}} (r_{12}l^{(2)^T})_x AU_h^n\psi^{(2)}(x,t^n)dx \\
&\quad \left. + \int_{I_j^{*,(2)}} r_{12}l^{(2)^T}F(x,t^n)\psi^{(2)}(x,t^n)dx\right)
\end{aligned}
\tag{3.20}
$$

where $\Delta t^n = t^{n+1} - t^n$. We compute the four integration terms of (3.20)

$$
\int_{I_j^{*,(1)}} r_{11}l^{(1)^T}U_h^n\psi^{(1),n}dx, \quad \int_{I_j^{*,(2)}} r_{12}l^{(2)^T}U_h^n\psi^{(2),n}dx,
$$

$$
\int_{\tilde{I}_j^{(1)}(t^n)} (r_{11}l^{(1)^T})_x AU_h^n\psi^{(1)}(x,t^n)dx, \quad \int_{\tilde{I}_j^{(2)}(t^n)} (r_{12}l^{(2)^T})_x AU_h^n\psi^{(2)}(x,t^n)dx
$$

highlighted in blue with U_h^n on background meshes subinterval-by-subinterval for mass conservation. Similarly, we can get $u_h^{2,n+1}$ on I_j.

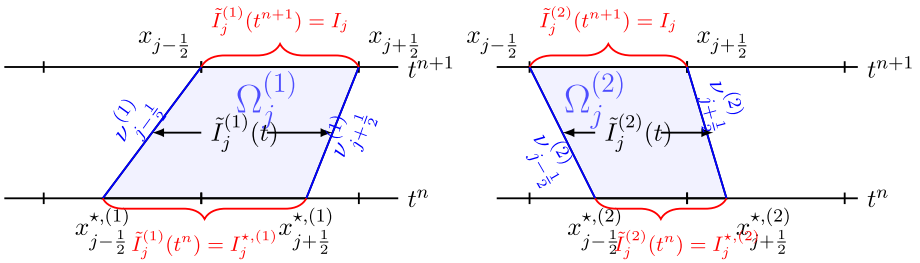

Fig. 2 Illustration for dynamic elements $\tilde{I}_j^{(1)}(t)$ (left) and $\tilde{I}_j^{(2)}(t)$ (right) of ELDG for the first and second characteristic families of the system (Color figure online)

(b2) For SSPRK2 method which is a trapezoid rule, we get $u_h^1(t^{(1)})$ from (3.20), then compute

$$\begin{aligned}
&\int_{I_j} u_h^{1,n+1}\Psi(x)dx \\
&= \int_{I_j^{*,(1)}} r_{11} l^{(1)^T} U_h^n \psi^{(1),n} dx + 0.5\Delta t L_{11}(U_h(t^{(1)}), t^{(1)}, I_j) \\
&\quad + \int_{I_j^{*,(2)}} r_{12} l^{(2)^T} U_h^n \psi^{(2),n} dx + 0.5\Delta t L_{12}(U_h(t^{(1)}), t^{(1)}, I_j),
\end{aligned} \tag{3.21}$$

where $t^{(1)} = t^{n+1}$, $u_h^1(t^{(1)})$ and $u_h^2(t^{(1)})$ are defined on background mesh I_j.

(b3) For general RK methods with intermediate stages, we will update intermediate RK solutions on background mesh as in [8]. For example, for a 2nd order mid point rule, it has an intermediate stage at $t^{(1)} = t^n + \frac{\Delta t}{2}$. We propose the following steps, also see Fig. 3.

A. We denote the dynamic domain tracking I_j from $t^{(1)}$ to t_n with speed $\nu_{j\pm\frac{1}{2}}^{(1)}$ at mesh point $x_{j\pm\frac{1}{2}}$ as $\tilde{I}_{j,(1)}^{(1)}(t)$, see the green domain in Fig. 3. $\tilde{I}_{j,(1)}^{(2)}(t)$ related to second characteristic is defined similarly. Then we can update $U_h(t^{(1)})$ on $\tilde{I}_{j,(1)}^{(1)}(t)$ and $\tilde{I}_{j,(1)}^{(2)}(t)$ from t^n to $t^{(1)}$ as in a forward-Euler method.

B. We update U_h^{n+1} on dynamic domain $\tilde{I}_j^{(1)}(t)$ and $\tilde{I}_j^{(2)}(t)$ from U_h^n with projection onto $I_j^{*,(1)}$ and $U_h(t^{(1)})$ with projection onto $\tilde{I}_{j,(1)}^{(1)}(t^{(1)})$.

Theorem 3.2 (Conservation) *The proposed fully discrete ELDG scheme with strong stability preserving Runge–Kutta (SSPRK) time discretization for (3.1) with $F = \mathbf{0}$ is locally conservative. In particular, given a ELDG solution $u_h(x, t^n) \in V_h^k$ with a periodic boundary condition, we have*

$$\sum_{i=1}^{N} \int_{I_j} U_h(x, t^{n+1})dx = \sum_{i=1}^{N} \int_{I_j} U_h(x, t^n)dx.$$

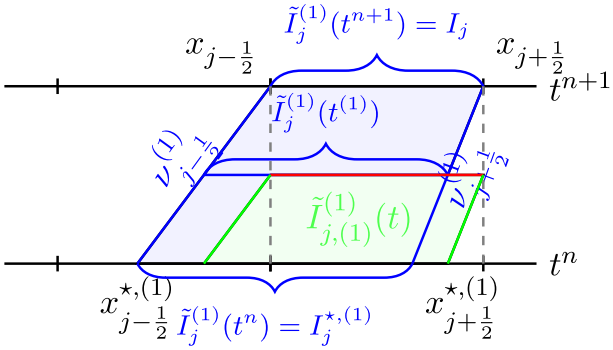

Fig. 3 Update RK intermediate solutions at the background mesh (red line) from the first characteristic family of a hyperbolic system

Proof We firstly consider the forward Euler time discretization. Taking $\Psi = 1$ and $F = \mathbf{0}$ in the scheme (3.20), we have

$$
\begin{aligned}
&\int_\Omega u_h^{1,n+1} dx = \sum_j \int_{I_j} u_h^{1,n+1} dx \\
&= \sum_j \left[\int_{I_j^{*,(1)}} r_{11} l^{(1)^T} U_h^n dx + \Delta t \left(-\widehat{f^{11}_{j+\frac{1}{2}}}(U_h^{(1)}(t^n)) + \widehat{f^{11}_{j-\frac{1}{2}}}(U_h^{(1)}(t^n)) \right.\right. \\
&\quad \left.\left. + \int_{I_j^{*,(1)}} (r_{11} l^{(1)^T})_x A U_h^n dx \right) \right] \\
&\quad + \sum_j \left[\int_{I_j^{*,(2)}} r_{12} l^{(2)^T} U_h^n dx + \Delta t \left(-\widehat{f^{12}_{j+\frac{1}{2}}}(U_h^{(2)}(t^n)) + \widehat{f^{12}_{j-\frac{1}{2}}}(U_h^{(2)}(t^n)) \right.\right. \\
&\quad \left.\left. + \int_{I_j^{*,(2)}} (r_{12} l^{(2)^T})_x A U_h^n dx \right) \right] \\
&= \sum_j \left(\int_{I_j^{*,(1)}} r_{11} l^{(1)^T} U_h^n dx + \int_{I_j^{*,(2)}} r_{12} l^{(2)^T} U_h^n dx \right) \\
&\quad + \Delta t \sum_j \left(\int_{I_j^{*,(1)}} (r_{11} l^{(1)^T})_x A U_h^n dx + \int_{I_j^{*,(2)}} (r_{12} l^{(2)^T})_x A U_h^n dx \right) \\
&= \int_\Omega (r_{11} l^{(1)^T} + r_{12} l^{(2)^T}) U_h^n dx + \Delta t \int_\Omega (r_{11} l^{(1)^T} + r_{12} l^{(2)^T})_x A U_h^n dx \\
&= \int_\Omega u_h^{1,n} dx,
\end{aligned}
\tag{3.22}
$$

which follows from the cancellation of unique fluxes at cell boundaries, $r_{11} l^{(1)^T} + r_{12} l^{(1)^T} = [1, 0]$ and (3.4) with integration in a subinterval-by-subinterval fashion. The conservation for the fully discrete ELDG scheme can be proved in a similar fashion. □

Remark 3.3 To maintain the mass-conservative property, the choice of eigenvectors $R(x)$ is not necessarily exact for ELDG scheme, as long as $R(x)$ and $R^{-1}(x)$ are a consistent pair

throughout the domain. We can also choose an approximation of exact eigenvectors if it is not easy to obtain.

Remark 3.4 Another version of non-conservative ELDG method, with localized eigen-decomposition, is presented in the Appendix A. It was our first native attempt in developing ELDG methods for hyperbolic system. The essential difference between the non-conservative method, compared to the conservative method, is the eigen-decomposition of characteristic variables, in particular the R matrix in Eq. (3.2) and the projection onto characteristic variables in Step (3) above. In the conservative method, the eigen-decompositions for the first and second characteristic families are consistent locally; whereas in the nonconservative method, such decomposition depends on the cell of consideration (index by i or j as elaborated below). Specifically, the space–time region of the first characteristic family $\Omega_j^{(1)}$ could overlap with the second-characteristic family of another space–time region $\Omega_i^{(2)}$ (with $i \neq j$). Such inconsistency could cause issues with mass conservation, as illustrated next in the numerical section. The numerical performance of the non-conservative method will serve as a comparison for the proposed scheme in the numerical section.

3.2 2D Linear Hyperbolic System

The solution for high-dimensional hyperbolic systems is given by means of a characteristic cone, rather than individual characteristic lines [15]. Numerically, characteristic Galerkin [19] or evolution Galerkin [1, 16, 17] methods have been proposed and developed to solve high dimensional hyperbolic systems. This method is constructed by taking into account information propagated in all bicharacteristic directions and involving integrals around the characteristic cone. However, the backward integrals over the mantle, involving intermediate times, limit both the accuracy and the stability of the resulting schemes. Thus the finite volume evolution Galerkin (FVEG) schemes are introduced, which is in a predictor–corrector plus finite volume framework to get higher accuracy. Even though the FVEG method can achieve high-order accuracy and stability with extra large step, the algorithm implementation is very complex for high-dimensional problems. In this paper, we use the dimensional splitting method for higher dimensional problem.

Consider a first order 2D linear hyperbolic system

$$U_t + (A(x, y)U)_x + (B(x, y)U)_y = 0, \quad (x, y) \in \Omega. \tag{3.23}$$

We assume that the computational domain Ω is rectangular, and it can be partitioned into rectangular meshes with each computational cell $\Omega_{ij} = [x_{i-\frac{1}{2}}, x_{i+\frac{1}{2}}] \times [y_{j-\frac{1}{2}}, y_{j+\frac{1}{2}}]$, where we use the piecewise Q^k tensor-product polynomial spaces. Then we extend ELDG algorithm to 2D problems via dimensional splitting [20].

1. We first locate $(k+1)^2$ tensor-product Gaussian nodes on cell $\Omega_{ij} : (x_{i,p}, y_{j,q}),\ p, q = 0, \ldots, k$. For example, see Fig. 4(left) for the case of $k = 3$.
2. Then, the Eq. (3.23) is split into two 1D hyperbolic problems based on the quadrature nodes in both $x-$ and $y-$ directions:

$$U_t + (A(x, y)U)_x = 0, \tag{3.24}$$

$$U_t + (B(x, y)U)_y = 0. \tag{3.25}$$

Based on a 1D ELDG formulation, the split Eqs. (3.24) and (3.25) are evolved via Strang splitting over a time step Δt as follows.

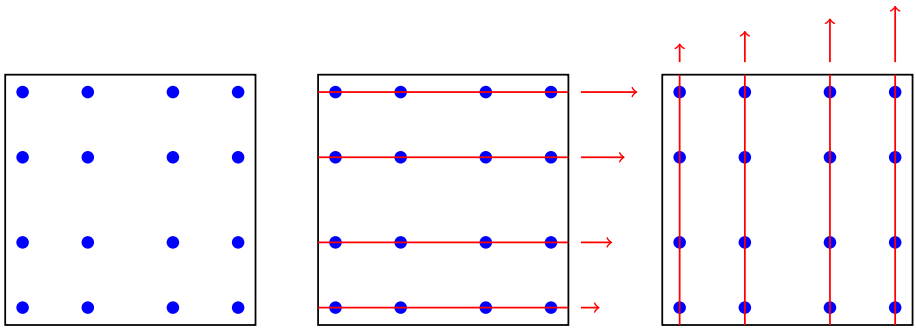

Fig. 4 Illustration of the 2D ELDG scheme via Strang splitting k = 3

- Evolve 1D Eq. (3.24) at different $y_{j,q}$ points for a half time-step $\Delta t/2$, see Fig. 4 (middle). For each $y_{j,q}$, the $(k+1)$ point values are mapped to a P^k polynomial per cell, then the 1D system (3.24) is evolved by the proposed ELDG scheme. Finally, we can map the evolved P^k polynomial back to the $(k+1)$ point values to update the solution.
- Evolve 1D system (3.25) at different $x_{i,p}$ points for a full time-step Δt as above, see Fig. 4(right).
- Evolve 1D system (3.24) at different $y_{j,q}$ points for another half time-step $\Delta t/2$.

The splitting 2D ELDG formulation maintains high order accuracy in space, extra large time stepping size with stability and conservation; and has a second order splitting error.

4 Numerical Results

In this section, we show numerical results of the proposed scheme for several linear strict hyperbolic systems including the wave equation, Maxwell equation and linearized shallow water equation. We set the time stepping size as $\Delta t = \frac{CFL}{a}\Delta x$ for 1D and $\Delta t = \frac{CFL}{\frac{a}{\Delta x}+\frac{b}{\Delta y}}$ for 2D, where a and b are maximum eigenvalues of coefficient matrixes in x- and y-directions respectively. We use the classical fourth order Runge–Kutta (RK4) method for time discretization. We study the following aspects: the spatial order of convergence by using small enough time stepping sizes, the temporal order of convergence and numerical stability under a large time stepping size by varying CFL for a fixed spatial mesh. We also study the spatial super-convergence of the post-processed solutions, so that temporal error will better dominate in the temporal convergence study. For the enhancement of spatial accuracy, we implement post-processing technique [5] to produce the post-processed solutions by convolving the ELDG solution with a suitable kernel consisting of B-splines at the final time.

4.1 1D Wave Equations

We consider the 1D wave equation:

$$u_{tt} = (a^2(x)u_x)_x + f(x,t). \tag{4.1}$$

For simplicity, we assume periodic boundary conditions, and the velocity field $a(x)$ is a continuous non-zero and periodic function of space. Defining $u^1 = u_t$ and $u^2 = u_x$, we can

rewrite (4.1) as a linear system (3.1) with

$$U = \begin{bmatrix} u^1 \\ u^2 \end{bmatrix}, \quad A(x) = \begin{bmatrix} 0 & -a^2(x) \\ -1 & 0 \end{bmatrix}, \quad F(x,t) = \begin{bmatrix} f(x,t) \\ 0 \end{bmatrix}.$$

Assume the eigen-decomposition of $A(x) = R(x)\Lambda R^{-1}(x)$ with $\Lambda(x) = diag(\lambda^{(1)}(x), \lambda^{(2)}(x))$, where the eigenvalues $\lambda^{(1)}(x) = a(x), \quad \lambda^{(2)}(x) = -a(x)$. The right eigenvectors and left eigenvectors are respectively

$$R(x) = \begin{bmatrix} r_{11}(x) & r_{12}(x) \\ r_{21}(x) & r_{22}(x) \end{bmatrix} = \begin{bmatrix} -a(x) & a(x) \\ 1 & 1 \end{bmatrix}, \quad R^{-1}(x) = \begin{bmatrix} l_j^{(1)^T} \\ l_j^{(2)^T} \end{bmatrix} = \begin{bmatrix} \frac{-1}{2a(x)} & \frac{1}{2} \\ \frac{1}{2a(x)} & \frac{1}{2} \end{bmatrix}. \quad (4.2)$$

Corresponding to (A.1) and (A.2) related to non-conservative ELDG scheme, we also have the following localized eigen-decomposition

$$R_j = \begin{bmatrix} r_j^{11} & r_j^{12} \\ r_j^{21} & r_j^{22} \end{bmatrix} = \begin{bmatrix} -a_j & a_j \\ 1 & 1 \end{bmatrix}, \quad R_j^{-1} = \begin{bmatrix} l_j^{(1)^T} \\ l_j^{(2)^T} \end{bmatrix} = \begin{bmatrix} \frac{-1}{2a_j} & \frac{1}{2} \\ \frac{1}{2a_j} & \frac{1}{2} \end{bmatrix}. \quad (4.3)$$

Example 4.1 (1D wave equation with constant coefficient). We consider the 1D wave Eq. (4.1) with constant coefficient $a(x) = 1$ and the source term $f(x,t) = 0$. The initial data is $u(x,0) = \sin(x), x \in [0, 2\pi]$ with periodic boundary condition. The exact solution is $u(x,t) = \sin(x+t)$. For the constant coefficient problem, if using exact characteristic velocity fields for space–time partition and exact eigenvectors, the proposed ELDG method is the same as SLDG, then it is unconditionally stable. Here we perturb the characteristic velocity $v^{(1)}_{j+\frac{1}{2}}$ in (3.6) at cell boundaries and/or $a(x)$ in (4.2) related to approximating eigenvectors to get ELDG, ELDG1, ELDG2 and ELDG3 schemes respectively. Similarly we implement the non-conservative ELDG methods denoted as NC ELDG, NC ELDG1, NC ELDG2 and NC ELDG3. Related parameters of these ELDG methods are given in Table 1.

Tables 2 and 3 report spatial accuracies of the ELDG, ELDG1, ELDG2 and ELDG3 methods for this example under the same time stepping size without and with post-processing technique. We can observe the optimal convergence rate $k+1$ and $2k+1$. We vary time stepping sizes, with fixed well-resolved spatial meshes, and plot error versus CFL in Figs. 5 and 6 for ELDG, ELDG1, ELDG2 and ELDG3 schemes without and with post-processed technique respectively, after a long time $T = 100$. The plots from post-processed ELDG schemes better show the fourth order temporal convergence. ELDG2 and ELDG3 perform comparably; they have a more restricted time step constraint than ELDG1. It indicates that, stability is affected by approximations of characteristic via the space–time partition and approximation of eigenvectors. We also note that, in both Figs. 5 and 6, the CFL allowed with stability (observed to be around 1) is much larger than that of the RK DG method which is $\frac{1}{2k+1}$. We observe similar performance of NC ELDG schemes in terms of the error and stability for this test; but skip presenting results to save space. Further, we verify the conservative property of the ELDG schemes are around machine precision and the non-conservative property of the NC ELDG schemes is presented in Fig. 7.

Example 4.2 We consider the wave Eq. (4.1) with a Gaussian initial condition

$$u^1 = \exp\left(-\frac{x^2}{0.005}\right), \quad u^2 = 0.$$

Table 1 The numerical parameters of various ELDG methods for $u_{tt} = u_{xx}$

Setting	ELDG	ELDG1	ELDG2	ELDG3
$\nu^{(1)}_{j+\frac{1}{2}}$ in (3.6), $\nu^{(2)}_{j+\frac{1}{2}} = -\nu^{(1)}_{j+\frac{1}{2}}$	1	$1 + \sin(x_j)\Delta x$	1	$1 + \sin(x_j)\Delta x$
$a(x)$ in (4.2)	1	1	$1 + \sin(x)\Delta x$	$1 + \sin(x)\Delta x$
Setting	NC ELDG	NC ELDG1	NC ELDG2	NC ELDG3
$\nu^{(1)}_{j+\frac{1}{2}}$ in (3.6), $\nu^{(2)}_{j+\frac{1}{2}} = -\nu^{(1)}_{j+\frac{1}{2}}$	1	$1 + \sin(x_j)\Delta x$	1	$1 + \sin(x_j)\Delta x$
a_j in (4.3)	1	1	$1 + \sin(x_j)\Delta x$	$1 + \sin(x_j)\Delta x$

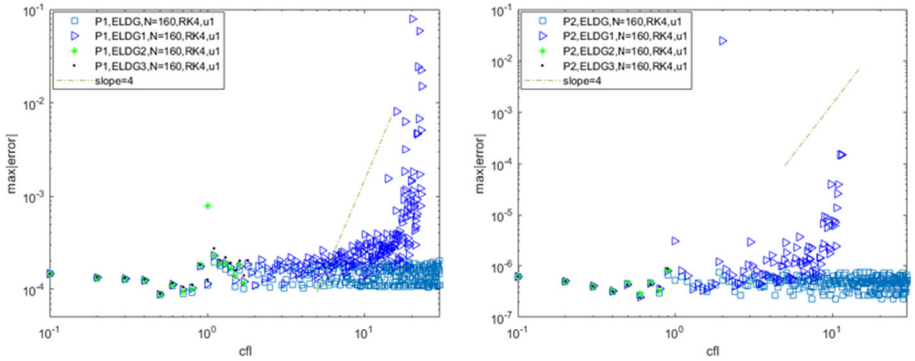

Fig. 5 The L^{∞} error versus CFL of various ELDG methods for 1D wave equation with the initial condition $u(x,0) = \sin(x)$. A long time simulation is performed with $T = 100$ and mesh size $N = 160$

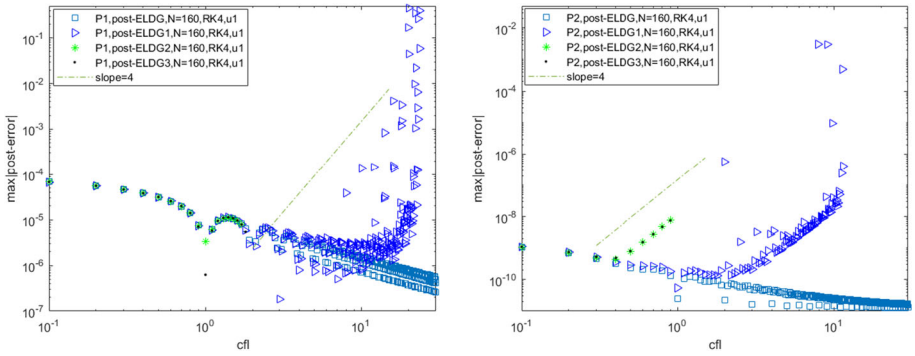

Fig. 6 The L^{∞} error versus CFL of various ELDG methods with post-processed technique for 1D wave equation with constant coefficient: $u_{tt} = u_{xx}$ with initial condition $u(x,0) = \sin(x)$. A long time simulation is performed with $T = 100$ and mesh size $N = 160$

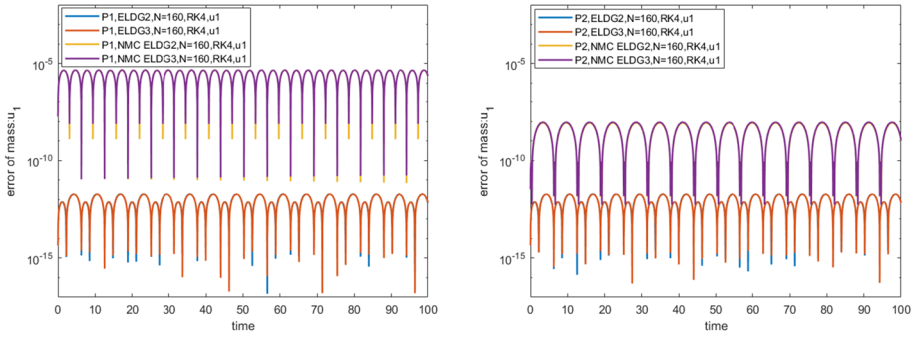

Fig. 7 The error of mass versus time of ELDG schemes for 1D wave equation and the initial condition $u(x,0) = \sin(x)$. A long time simulation $T = 100$ is performed with meshes $N = 160$, $CFL = 0.1$ and RK4 time discretization. In the legend "NMC" is for the non-conservative method

Table 2 1D wave equation with the initial condition $u(x,0) = \sin(x)$ at $T = 1$

Mesh	L^1 Error P^1 ELDG	Order	L^1 Error P^1 ELDG1	Order	L^1 Error P^1 ELDG2	Order	L^1 Error P^1 ELDG3	Order
20	2.54E−03	–	2.42E−03	–	2.55E−03	–	2.49E−03	–
40	6.18E−04	2.03	5.97E−04	2.02	6.18E−04	2.04	5.99E−04	2.06
80	1.58E−04	1.96	1.55E−04	1.94	1.58E−04	1.96	1.55E−04	1.95
160	3.66E−05	2.11	3.62E−05	2.10	3.66E−05	2.11	3.62E−05	2.10
	P^2 ELDG		P^2 ELDG1		P^2 ELDG2		P^2 ELDG3	
20	5.92E−05	–	6.91E−05	–	6.01E−05	–	7.02E−05	–
40	7.48E−06	2.99	7.83E−06	3.14	7.49E−06	3.00	7.81E−06	3.17
80	9.17E−07	3.03	9.29E−07	3.08	9.17E−07	3.03	9.29E−07	3.07
160	1.17E−07	2.97	1.18E−07	2.98	1.17E−07	2.97	1.18E−07	2.98

We use $CFL = 0.3$ and $CFL = 0.18$ with RK4 time discretization for all P^1 and P^2 respectively. The error for only $u^1 = u_t$ was shown in this table

Table 3 1D wave equation with the initial condition $u(x,0) = \sin(x)$ at $T = 1$

Mesh	L^1 Error P^1 ELDG	Order	L^1 Error P^1 ELDG1	Order	L^1 Error P^1 ELDG2	Order	L^1 Error P^1 ELDG3	Order
20	2.26E−04	–	2.49E−04	–	2.38E−04	–	2.39E−04	–
40	2.36E−05	3.26	2.40E−05	3.38	2.40E−05	3.31	2.35E−05	3.35
80	2.66E−06	3.15	2.64E−06	3.18	2.67E−06	3.16	2.62E−06	3.16
160	3.15E−07	3.08	3.11E−07	3.08	3.15E−07	3.09	3.11E−07	3.08
	P^2 ELDG		P^2 ELDG1		P^2 ELDG2		P^2 ELDG3	
20	2.15E−06	–	2.27E−06	–	2.19E−06	–	2.28E−06	–
40	3.63E−08	5.89	3.86E−08	5.87	3.67E−08	5.90	3.89E−08	5.87
80	6.40E−10	5.83	6.79E−10	5.83	6.46E−10	5.83	6.84E−10	5.83
160	1.27E−11	5.66	1.33E−11	5.68	1.28E−11	5.66	1.34E−11	5.68

We use $CFL = 0.3$ and $CFL = 0.18$ with RK4 time discretization and post-processed technique for all P^1 and P^2 respectively. The error with post-processed technique for only $u^1 = u_t$ was shown in this table

The computational domain is $[-1, 1]$ with the periodic boundary conditions. The exact solutions $u^1 = 0.5\left[\exp\left(-\frac{(x+t)^2}{0.005}\right) + \exp\left(-\frac{(x-t)^2}{0.005}\right)\right]$ and $u^2 = 0.5\left[\exp\left(-\frac{(x+t)^2}{0.005}\right) - \exp\left(-\frac{(x-t)^2}{0.005}\right)\right]$ are the superposition of two Gaussian functions with a periodic extensions. We plot the solution u^1 from ELDG3 with P^1 and P^2 numerical solutions at time $T = 50.5$ in Fig. 8. We can observed that there is no significant phase difference with a long time simulation, meanwhile the dissipation can be improved by the mesh refinement and higher order spatial approximation. Note that the CFL number we use here is much larger than the upper bound for Eulerian RK DG methods.

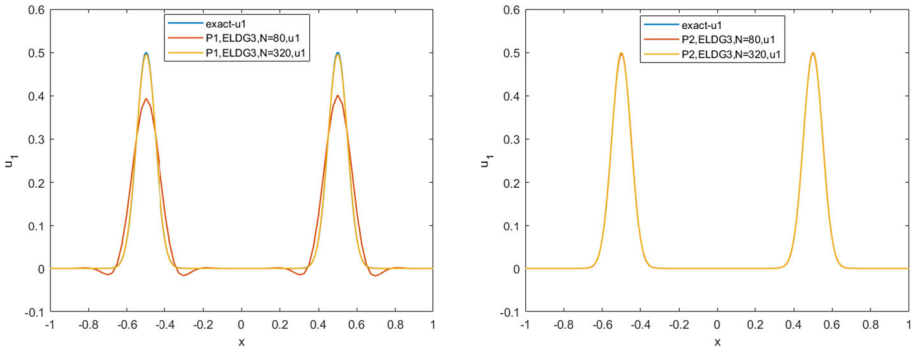

Fig. 8 Plots of the exact and numerical solutions u_1 at time $T = 50.5$ of ELDG3 scheme for solving $u_{tt} = u_{xx}$ with Gaussian function initial condition. The mesh size of $N = 80$ and $N = 320$ are used. Left: $k = 1$ ELDG3 with $CFL = 1.5$. Right: $k = 2$ ELDG3 with $CFL = 0.9$

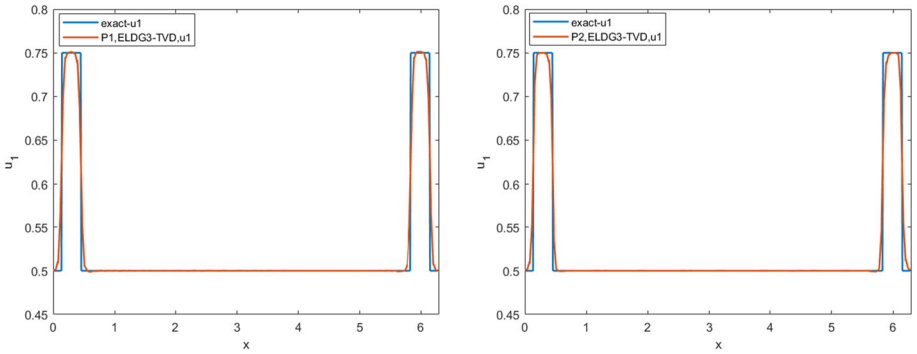

Fig. 9 Plots of the numerical solutions u_1 of ELDG3 scheme with TVD limiter for the wave equation with step function initial condition. The final integration time T is 2.85. The mesh of 160 is used. Left: $k = 1$ ELDG3+TVDlimiter with $CFL = 1.5$. Right: $k = 2$ ELDG3+TVDlimiter with $CFL = 0.9$

Example 4.3 We consider the wave Eq. (4.1) on $[0, 2\pi]$ with the periodic boundary conditions and the following discontinuous initial condition

$$u_0^1(x) = \begin{cases} 1, & \text{if } 0.95\pi \le x \le 1.05\pi, \\ 0.5, & \text{otherwise,} \end{cases} \qquad u_0^2(x) = 1. \tag{4.4}$$

The exact solutions u^1 and u^2 are discontinuous piecewise constants with moving discontinuities. It is a challenging test for controlling oscillations around discontinuities. We adopt a simple TVD limiter on background mesh at each RK stages with M = 0 in [6] for all schemes. As shown in Fig. 5, the CFL constraint with stability is slightly less than 1 for ELDG3 scheme. We plot the numerical solutions u_1 of ELDG3 scheme with P^1 and P^2, $CFL = 0.9$ in Fig. 9. It is found that oscillations are well controlled with the TVD limiter and ELDG method performs well for large time stepping size. Moreover, we track the conservation of ELDG methods, in comparison to the NC ELDG methods and present results in Fig. 10. It shows that the ELDG schemes maintain the conservation at the level of machine error, while the NC ELDG schemes do not.

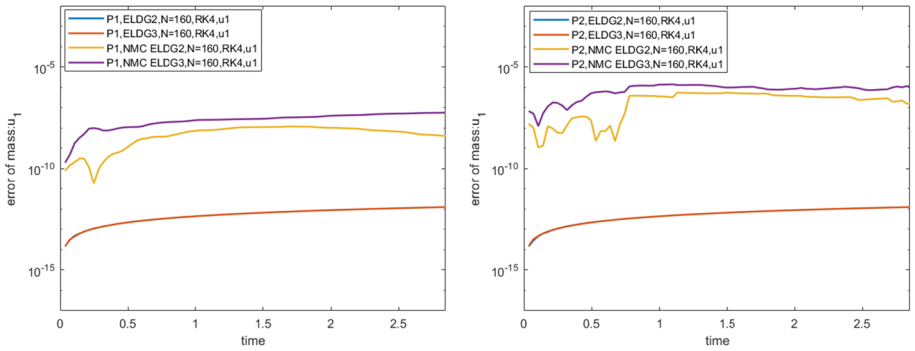

Fig. 10 The error of mass versus time of various ELDG methods with TVD limiter for 1D wave equation. $T = 2.85$, $N = 160$, $CFL = 0.9$ and RK4 time discretization are performed for the simulation

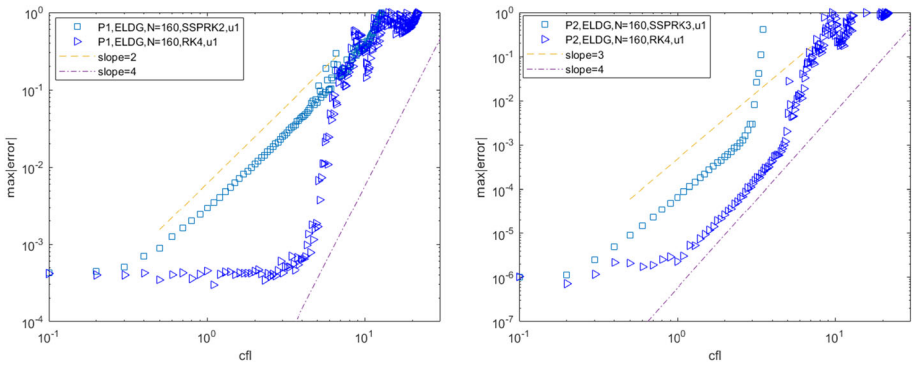

Fig. 11 The L^∞ error versus CFL of ELDG method for Example 4.4. $T = 1$. $\Delta t = CFL\Delta x$

Example 4.4 (1D wave equation with variable coefficient and source term). We consider the 1D wave Eq. (4.1) with variable coefficient $a(x) = 2 + \sin(x)$ and exact solution $u(x, t) = \sin(x - 2t)$ is periodic on $[0, 2\pi]$. The source term is $f(x, t) = -4\sin(x - 2t) + \sin(x - 2t)(2 + \sin(x))^2 - 2(2 + \sin(x))\cos(x)\cos(x - 2t)$. For computation, we choose mesh velocity $v^{(1)}_{j+\frac{1}{2}} = a(x_{j+\frac{1}{2}})$, $v^{(2)}_{j+\frac{1}{2}} = -v^{(1)}_{j+\frac{1}{2}}$ and exact eigenvectors with $a(x) = 2 + \sin(x)$ in (4.2).

The expected optimal spatial accuracies of the ELDG methods without and with post-processing technique are shown in Tables 4 and 5 respectively. In Figs. 11 and 12, we plot the L^∞ error versus CFL of EL DG methods without and with post-processing technique respectively. The following observations are made: (1) The high order accuracy of the RK method reduce the error magnitude when large time stepping size is used; (2) The ELDG methods with RK4 time discretization perform well around and before $CFL = 1$, which is well above the stability constraint of the RKDG method $1/(2k+1)$ for P^k approximations. (3) After $CFL = 1$ and before stability constraint of the method, the temporal convergence order is observed to be consistent with the order of RK discretization; (4) The ELDG methods with post-processing technique have smaller error magnitute than those without post-processing.

Table 4 Example 4.4

Mesh	L^1 Error	Order	L^2 Error	Order	L^∞ Error	Order
P^1						
20	5.20E−03	–	6.70E−03	–	2.39E−02	–
40	1.32E−03	1.98	1.74E−03	1.94	6.54E−03	1.87
80	3.28E−04	2.00	4.40E−04	1.99	1.68E−03	1.96
160	8.11E−05	2.02	1.09E−04	2.01	4.16E−04	2.01
P^2						
20	1.16E−04	–	1.61E−04	–	5.48E−04	–
40	1.48E−05	2.97	2.01E−05	3.00	6.70E−05	3.03
80	1.88E−06	2.98	2.46E−06	3.03	7.84E−06	3.10
160	2.31E−07	3.02	3.13E−07	2.98	1.04E−06	2.91

$T = 1$. We use $CFL = 0.1$ for P^1 and P^2 with RK4 time discretization. The error for only $u^1 = u_t$ was shown in this table

Table 5 Example 4.4

Mesh	L^1 Error	Order	L^2 Error	Order	L^∞ Error	Order
P^1						
20	9.10E−04	–	1.07E−03	–	1.91E−03	–
40	1.07E−04	3.09	1.26E−04	3.09	2.26E−04	3.08
80	1.29E−05	3.05	1.53E−05	3.05	2.75E−05	3.04
160	1.58E−06	3.02	1.88E−06	3.02	3.39E−06	3.02
P^2						
20	5.34E−06	–	6.39E−06	–	1.56E−05	–
40	8.95E−08	5.90	1.03E−07	5.96	2.82E−07	5.79
80	1.73E−09	5.69	1.94E−09	5.73	3.32E−09	6.41
160	6.62E−11	4.71	7.59E−11	4.67	1.46E−10	4.51

$T = 1$. We use $CFL = 0.1$ for P^1 and P^2 with post-processed technique and RK4. The error for only $u^1 = u_t$ was shown in this table

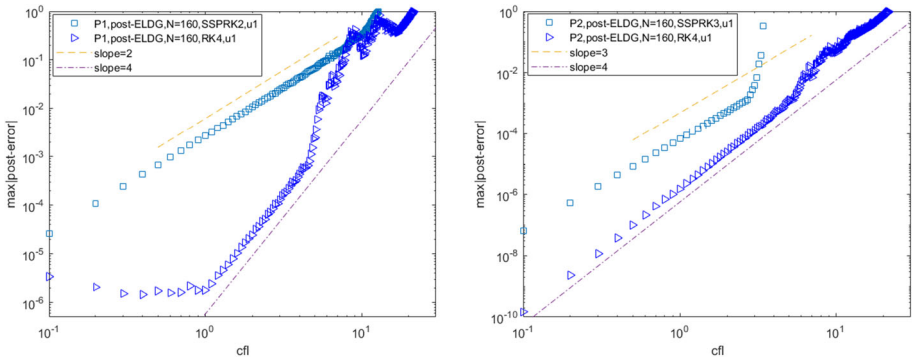

Fig. 12 The L^∞ error versus CFL of ELDG method with post-processed technique for Example 4.4. $T = 1$. $\Delta t = CFL\Delta x$

Table 6 Example 4.5

Mesh	L^1 error	Order	L^2 error	Order	L^∞ error	Order
Q^1						
20^2	8.03E−04	–	9.47E−04	–	1.85E−03	–
40^2	2.16E−04	1.89	2.50E−04	1.92	4.56E−04	2.02
80^2	5.57E−05	1.96	6.40E−05	1.97	1.13E−04	2.02
160^2	1.43E−05	1.96	1.64E−05	1.97	2.84E−05	1.99
Q^2						
20^2	1.70E−04	–	1.90E−04	–	3.12E−04	–
40^2	2.21E−05	2.95	2.47E−05	2.94	4.14E−05	2.91
80^2	2.75E−06	3.00	3.08E−06	3.00	5.21E−06	2.99
160^2	3.38E−07	3.02	3.80E−07	3.02	6.45E−07	3.01

Q^k ELDG methods (k = 1, 2) with RK4 and 4th time discretization methods for (4.5) with the smooth initial condition at T = 1. $CFL = 0.1$

4.2 2D Wave Equations

Example 4.5 (Two-dimensional linear system with constant coefficient matrices). The second order wave equation $u_{tt} = u_{xx} + u_{yy}$ can be written as the following first order linear hyperbolic system:

$$\begin{cases} \begin{pmatrix} u \\ v \end{pmatrix}_t + \begin{pmatrix} -1 & 0 \\ 0 & 1 \end{pmatrix} \begin{pmatrix} u \\ v \end{pmatrix}_x + \begin{pmatrix} 0 & -1 \\ -1 & 0 \end{pmatrix} \begin{pmatrix} u \\ v \end{pmatrix}_y = \begin{pmatrix} 0 \\ 0 \end{pmatrix}, \\ u(x, y, 0) = \frac{1}{2\sqrt{2}} \sin(x + y) - \frac{1}{2\sqrt{2}} \cos(x + y), \\ v(x, y, 0) = \frac{\sqrt{2}-1}{2\sqrt{2}} \sin(x + y) + \frac{\sqrt{2}+1}{2\sqrt{2}} \cos(x + y) \end{cases} \tag{4.5}$$

with period boundary conditions in both x and y directions. The exact solution is

$$\begin{cases} u(x, y, t) = \frac{1}{2\sqrt{2}} \sin(x + y + \sqrt{2}t) - \frac{1}{2\sqrt{2}} \cos(x + y - \sqrt{2}t), \\ v(x, y, t) = \frac{\sqrt{2}-1}{2\sqrt{2}} \sin(x + y + \sqrt{2}t) + \frac{\sqrt{2}+1}{2\sqrt{2}} \cos(x + y - \sqrt{2}t). \end{cases} \tag{4.6}$$

We notice that the two matrices in Eq. (4.5) don't commute, thus the linear system can not be reduced to 2D scalar problems. We test accuracy for Q^k ELDG methods with RK4 and 4th order dimensional splitting method [23, 24] at $T = 1$ for $k = 1, 2$ with $CFL = 0.1$ in Table 6. As expected, the $(k + 1)$th order convergence is observed for these methods. We plot the L^∞ error versus CFL of ELDG methods with Q^1 (left) and Q^2 (right) polynomial spaces for this case with Strang splitting and 4th order splitting in Fig. 13, which shows that second and forth order splitting errors are dominant when time-stepping sizes are large enough. The CFL constraint with stability for ELDG method is larger than that for general RKDG method when high order time discretization is applied.

Example 4.6 (Two-dimensional linear system with variable coefficient matrices). The second order wave equation $u_{tt} = (a^2(x, y)u_x)_x + (b^2(x, y)u_y)_y$ can be written as the following first order linear hyperbolic system by taking $u_1 = u_t,\ u_2 = u_x,\ u_3 = u_y$:

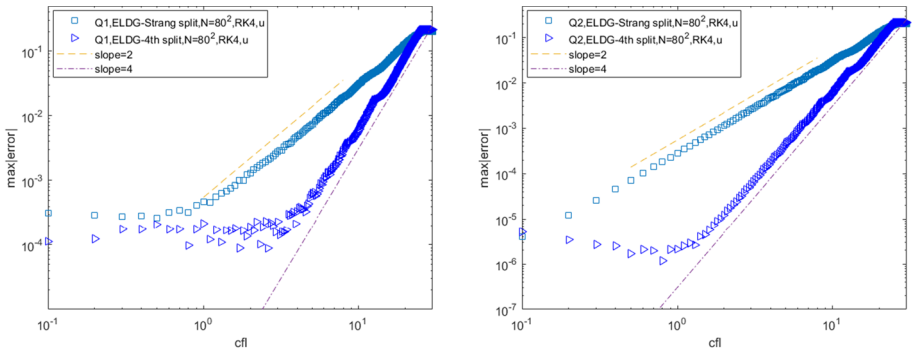

Fig. 13 Example 4.5. The L^∞ error versus CFL of ELDG method with Strang splitting and 4th splitting, RK4 time discretization for (4.5) at $T = 1$

$$\left\{\begin{pmatrix} u_1 \\ u_2 \\ u_3 \end{pmatrix}_t + \left[\begin{pmatrix} 0 & -(a(x,y))^2 & 0 \\ -1 & 0 & 0 \\ 0 & 0 & 0 \end{pmatrix}\begin{pmatrix} u_1 \\ u_2 \\ u_3 \end{pmatrix}\right]_x + \left[\begin{pmatrix} 0 & 0 & -(b(x,y)^2) \\ 0 & 0 & 0 \\ -1 & 0 & 0 \end{pmatrix}\begin{pmatrix} u_1 \\ u_2 \\ u_3 \end{pmatrix}\right]_y = \begin{pmatrix} 0 \\ 0 \\ 0 \end{pmatrix}. \tag{4.7}$$

We consider the system (4.7) with the initial condition

$$\begin{cases} u_1(x, y, 0) = 2\cos(x + y), \\ u_2(x, y, 0) = \cos(x + y), \\ u_3(x, y, 0) = \cos(x + y), \end{cases} \tag{4.8}$$

where $a(x, y) = 1+0.5\sin(x+y), b(x, y) = \sqrt{(4 - (1 + 0.5\sin(x + y))^2)}$ and the boundary condition is periodic in both x and y directions. The exact solution is

$$\begin{cases} u_1(x, y, t) = 2\cos(x + y + 2t), \\ u_2(x, y, t) = \cos(x + y + 2t), \\ u_3(x, y, t) = \cos(x + y + 2t). \end{cases} \tag{4.9}$$

We report the spatial accuracy of Q^k ELDG methods in Table 7. The expected optimal convergence is observed. We plot the L^∞ error versus CFL of ELDG methods in Fig. 14. The ELDG methods perform as well as that for the linear system with constant coefficient matrices, and the CFL allowed with stability is much larger than that of the RKDG method.

4.3 2D Maxwell Equations

Example 4.7 Consider the 2D Maxwell equations:

$$\begin{cases} \frac{\partial H_x}{\partial t} + \frac{\partial E_z}{\partial y} = 0, \\ \frac{\partial H_y}{\partial t} - \frac{\partial E_z}{\partial x} = 0, \\ \frac{\partial E_z}{\partial t} - \frac{\partial H_y}{\partial x} + \frac{\partial H_x}{\partial y} = 0, \end{cases} \tag{4.10}$$

Table 7 Example 4.6

Mesh	L^1 Error	Order	L^2 Error	Order	L^∞ Error	Order
Q^1						
20^2	1.89E−03	–	2.46E−03	–	5.29E−03	–
40^2	4.58E−04	2.05	6.01E−04	2.03	1.26E−03	2.07
80^2	1.13E−04	2.02	1.50E−04	2.00	3.10E−04	2.02
160^2	2.81E−05	2.01	3.73E−05	2.01	7.67E−05	2.01
Q^2						
20^2	2.95E−04	–	3.66E−04	–	8.43E−04	–
40^2	4.06E−05	2.86	4.91E−05	2.90	1.01E−04	3.07
80^2	5.15E−06	2.98	6.20E−06	2.99	1.30E−05	2.95
160^2	6.49E−07	2.99	7.80E−07	2.99	1.63E−06	2.99

Q^k ELDG methods (k = 1, 2) with RK4 and 4th splitting time discretization methods for (4.7) with the smooth initial condition at T = 0.1, $CFL = 0.1$

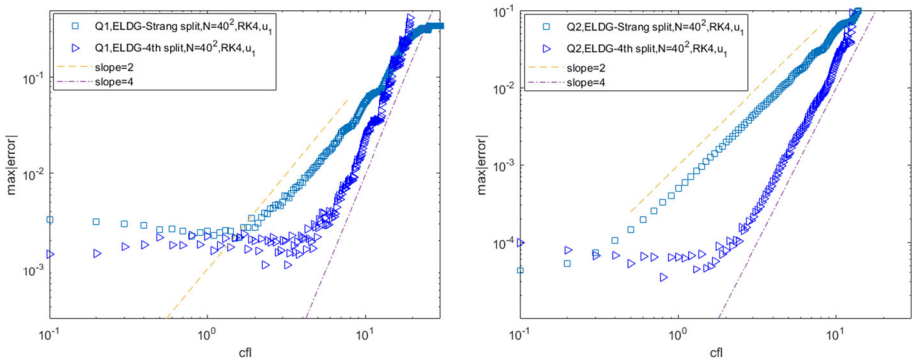

Fig. 14 Example 4.6. The L^∞ error versus CFL of ELDG method with Strang splitting and 4th splitting, RK4 time discretization for (4.7). $T = 1$, mesh size 40^2

which is a linear hyperbolic system and can be written as

$$U_t + AU_x + BU_y = 0, \tag{4.11}$$

where

$$U = \begin{bmatrix} u_1 \\ u_2 \\ u_3 \end{bmatrix} = \begin{bmatrix} E_z \\ H_x \\ H_y \end{bmatrix}, \quad A = \begin{bmatrix} 0 & 0 & -1 \\ 0 & 0 & 0 \\ -1 & 0 & 0 \end{bmatrix}, \quad B = \begin{bmatrix} 0 & 1 & 0 \\ 1 & 0 & 0 \\ 0 & 0 & 0 \end{bmatrix}.$$

We take the computational domain $[-1, 1] \times [-1, 1]$ with periodic boundary condition and the Gaussian function initial condition:

$$\begin{cases} u_1(x, y, 0) = \exp(-\frac{x^2+y^2}{0.005}), \\ u_2(x, y, 0) = 0, \\ u_3(x, y, 0) = 0. \end{cases} \tag{4.12}$$

For this example, we show the numerical ELDG Q^2 solution u_1 at times $T = 0.5, 1, 1.5, 2$ in Fig. 15.

4.4 2D Linearized Shallow Water Equations

We consider the following linearized shallow water system from oceanic shallow water model [11]:

$$\frac{\partial}{\partial t}\begin{bmatrix}\phi\\ \Phi u\\ \Phi v\end{bmatrix}+\frac{\partial}{\partial x}\begin{bmatrix}\Phi u\\ \Phi\phi\\ 0\end{bmatrix}+\frac{\partial}{\partial y}\begin{bmatrix}\Phi v\\ 0\\ \Phi\phi\end{bmatrix}=\begin{bmatrix}0\\ f\Phi v-r\Phi u+\frac{\tau_x}{\rho}\\ -f\Phi u-r\Phi v+\frac{\tau_y}{\rho}\end{bmatrix}, \tag{4.13}$$

where ϕ is the geopotential height, $\Phi > 0$ is a constant mean flow geopotential height, (u, v) is the perturbed velocity, $\gamma \geq 0$ is the bottom friction, (τ_x, τ_y) is the wind stress, ρ is the water density, and $f = f_0 + \beta(y - y_m)$ is the Coriolis parameter, where f_0, β, y_m are constants. The linearized shallow water equations is a linear hyperbolic system

$$U_t + AU_x + BU_y = F \text{ in } \Omega, \tag{4.14}$$

where

$$U=\begin{bmatrix}\phi\\ \Phi u\\ \Phi v\end{bmatrix},\quad A=\begin{bmatrix}0&1&0\\ \Phi&0&0\\ 0&0&0\end{bmatrix},\quad B=\begin{bmatrix}0&0&1\\ 0&0&0\\ \Phi&0&0\end{bmatrix},\quad F=\begin{bmatrix}0\\ f\Phi v-\gamma\Phi u+\frac{\tau_x}{\rho}\\ -f\Phi u-\gamma\Phi v+\frac{\tau_y}{\rho}\end{bmatrix}.$$

Example 4.8 We take $\Phi = 1$, $f = 0, \gamma = 0$, and $(\tau_x, \tau_y) = \mathbf{0}$, which implies $F = \mathbf{0}$. The computational domain Ω is taken as $[-1, 1] \times [-1, 1]$ with periodic boundary condition and the discontinuous initial condition:

$$\begin{cases}\phi(x, y, 0) = \begin{cases}1, & \text{if } \ y \geq x,\\ 0.5, & \text{otherwise,}\end{cases}\\ u(x, y, 0) = 1,\\ v(x, y, 0) = 1.\end{cases} \tag{4.15}$$

We use TVD limiter and show the numerical ELDG Q^2 solution (ϕ, u, v) at times $T = 0.5$ in Fig. 16 with $CFL = 1$. Stable and accurate results are observed.

Example 4.9 We also consider the linear Kelvin wave by taking $\Phi = 1$, $f_0 = y_m = 0, \beta = 1$, $\gamma = 0$, and $(\tau_x, \tau_y) = \mathbf{0}, F = [0, yv, -yu]^T$. The computational domain Ω is $[-10, 10] \times [-5, 5]$ with periodic boundary condition. We consider the following exact solution:

$$\begin{cases}\phi = 1 + \exp\left(-\frac{y^2}{2}\right)\exp\left(-\frac{(x+5-t)^2}{2}\right),\\ u = \exp\left(-\frac{y^2}{2}\right)\exp\left(-\frac{(x+5-t)^2}{2}\right),\\ v = 0.\end{cases} \tag{4.16}$$

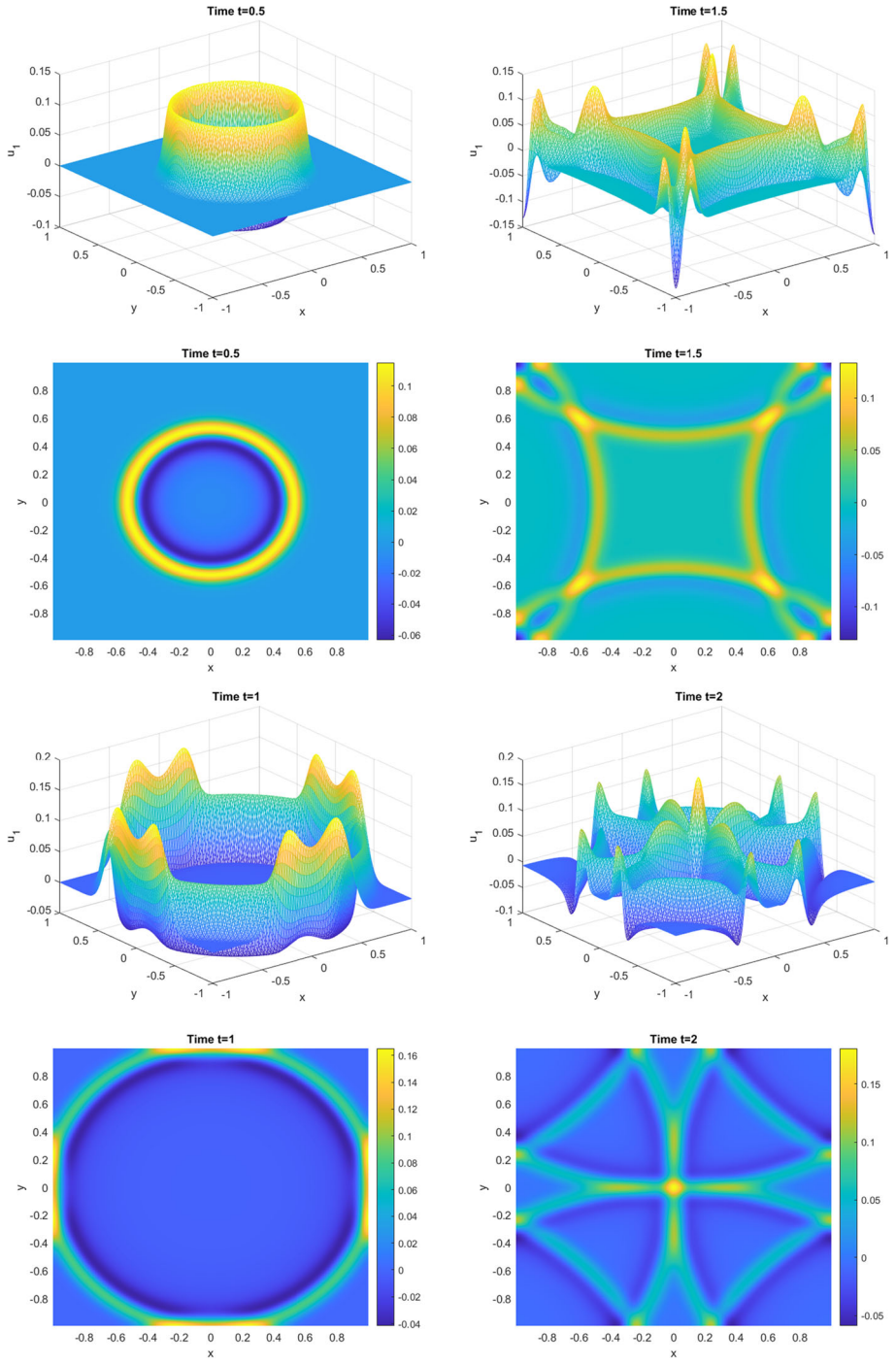

Fig. 15 Plots of the ELDG numerical solutions $u_1 = E_z$ and their contour plots at $T = 0.5, 1, 1.5, 2$ for 2D Maxwell Eq. (4.11) with Gaussian function initial condition. The mesh of 80×80 is used with 4th splitting method and RK4 time discretization, $CFL = 1$

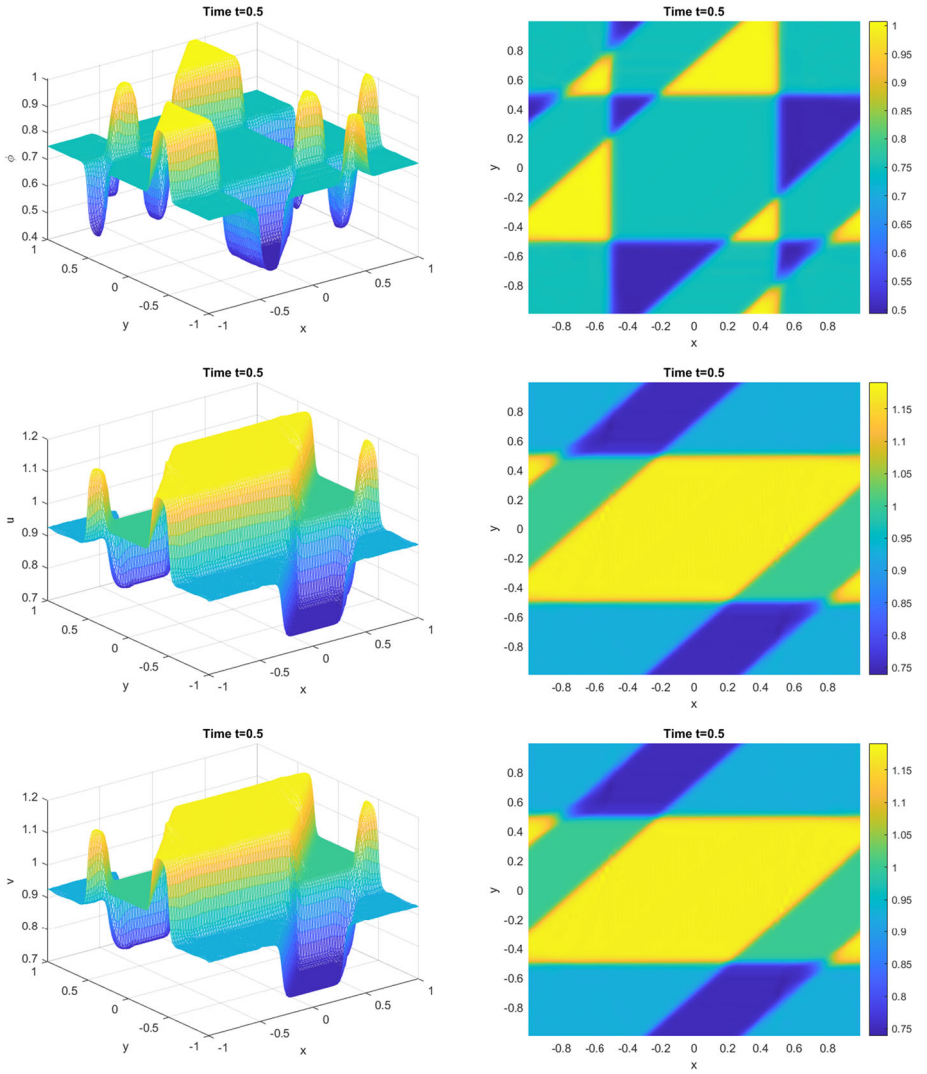

Fig. 16 Example 4.8. Plots of the ELDG Q^2 numerical solutions (ϕ, u, v) (from top to bottom) and their contour plots at $T = 0.5$. The mesh is 80×80; 4th splitting method and RK4 time discretization with $CFL = 1$ is used

We split the system as the following 1D system for stability

$$\begin{aligned} \frac{\partial}{\partial t}\begin{bmatrix}\phi\\ u\\ v\end{bmatrix} + \begin{bmatrix}0&1&0\\1&0&0\\0&0&0\end{bmatrix}\frac{\partial}{\partial x}\begin{bmatrix}\phi\\ u\\ v\end{bmatrix} &= \begin{bmatrix}0\\ yv\\ -yu\end{bmatrix}, \\ \frac{\partial}{\partial t}\begin{bmatrix}\phi\\ u\\ v\end{bmatrix} + \begin{bmatrix}0&0&1\\0&0&0\\1&0&0\end{bmatrix}\frac{\partial}{\partial y}\begin{bmatrix}\phi\\ u\\ v\end{bmatrix} &= \begin{bmatrix}0\\0\\0\end{bmatrix}. \end{aligned} \tag{4.17}$$

Table 8 Example 4.9

Mesh	L^1 Error	Order	L^2 Error	Order	L^∞ Error	Order
Q^1						
20^2	1.06E−03	–	4.06E−03	–	4.59E−02	–
40^2	2.24E−04	2.25	8.42E−04	2.27	9.95E−03	2.20
80^2	5.42E−05	2.05	1.96E−04	2.10	2.15E−03	2.21
160^2	1.35E−05	2.01	4.82E−05	2.03	4.91E−04	2.13
Q^2						
20^2	1.27E−04	–	4.64E−04	–	4.81E−03	–
40^2	1.95E−05	2.71	7.04E−05	2.72	6.14E−04	2.97
80^2	2.64E−06	2.89	9.67E−06	2.86	8.61E−05	2.83
160^2	3.45E−07	2.94	1.24E−06	2.97	1.09E−05	2.98

We take $CFL = 1.0$ and use Q^k ELDG methods ($k = 1, 2$) with RK4 and 4th splitting time discretization methods at $T = 1$. The error for only ϕ was shown in this table

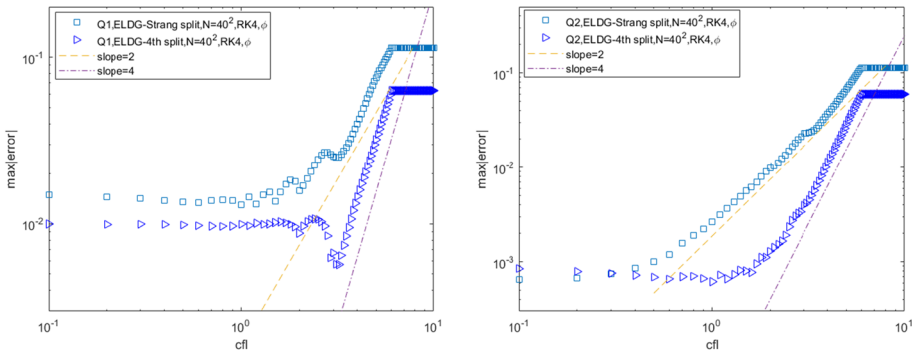

Fig. 17 Example 4.9. The L^∞ error versus CFL of ELDG method with Strang splitting and 4th splitting, RK4 time discretization with $T = 1$, mesh size 40^2

We take $CFL = 1.0$ and use Q^k ELDG methods ($k = 1, 2$) with RK4 and 4th splitting time discretization methods for this example. The error table is shown in Table 8, where the optimized convergence rate is observed. We also show the L^∞ error versus CFL of ELDG method with Strang splitting and 4th splitting, RK4 time discretization in Fig. 17. For this system, the total energy $E_{tot}(t) = \frac{1}{2}(||\phi||^2 + ||u||^2 + ||v||^2)$ should be preserved. Figure 18 shows that the ELDG method preserves the total energy to very high precision (the relative error is less than 10^{-5} for Q^1 and 10^{-8} for Q^2).

5 Conclusion

In this paper, we have developed a conservative Eulerian–Lagrangian discontinuous Galerkin (ELDG) method for linear hyperbolic systems. The new framework tracks the information of each characteristic family by the corresponding characteristic region, and these components are recombined in a conservative fashion. The method is shown to be stable under larger

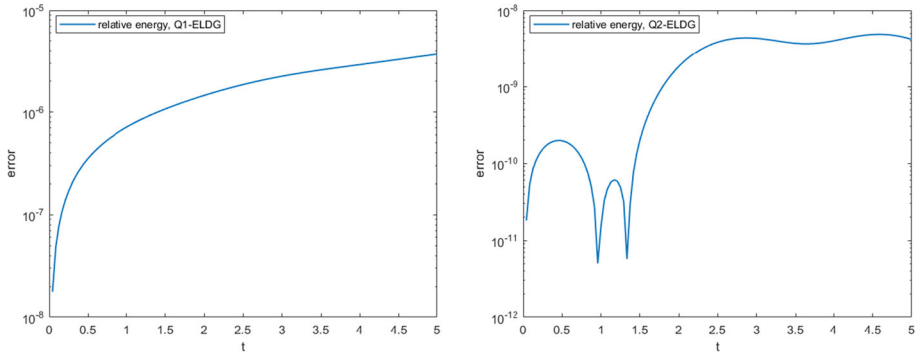

Fig. 18 Example 4.9. The time evolution of the relative energy $|(E_{tot}(t) - E_{tot}(0))/E_{tot}(0)|$ of Q^1 and Q^2 ELDG method with 4th splitting, RK4 time discretization with $CFL = 1$ and mesh size 160^2

time stepping constraints than the corresponding Eulerian RK DG methods. The methods are tested via extensive numerical experiments for 1D and 2D linear hyperbolic problems. Future works include further theoretic development and extension to general nonlinear hyperbolic problems.

Funding Research of the first author is supported by the Centre Henri Lebesgue, program ANR-11-LABX-0020-0 and the Brittany council. Research of the second author is supported by NSF Grants NSF-DMS-1818924 and 2111253, Air Force Office of Scientific Research FA9550-22-1-0390 and Department of Energy DE-SC0023164.

Data Availability The datasets and source code generated and analyzed during the current study are available in the repository https://github.com/xuehong05/conservativeELDGforlinearhyperbolic-system.

A Appendix A: Non-conservative ELDG Scheme

In this part, we formulate the scheme by a localized characteristic field. In particular, a piecewise constant a_j approximating $a(x)$ in (3.3) is defined on I_j, and the corresponding

$$R_j \doteq \left[r_j^{(1)} \mid r_j^{(2)}\right] = \begin{bmatrix} r_j^{11} & r_j^{12} \\ r_j^{21} & r_j^{22} \end{bmatrix} \tag{A.1}$$

and

$$R_j^{-1} \doteq \begin{bmatrix} {l_j^{(1)}}^T \\ {l_j^{(2)}}^T \end{bmatrix} \tag{A.2}$$

Define ${l_j^{(1)}}^T$ is locally defined on $\Omega_j^{(1)}$ approximating ${l^{(1)}}^T(x)$. For simplicity, we only present the first order ELDG scheme. Take the vector product of ${l_j^{(1)}}^T$ from left with (3.1), we have a scalar equation

$${l_j^{(1)}}^T (U_t + (A(x)U)_x) = {l_j^{(1)}}^T F(x,t). \tag{A.3}$$

Next, integrating over the space–time interval $\tilde{I}_j^{(1)}(t)$, then we have

$$\begin{aligned}\frac{d}{dt}\int_{\tilde{I}_j^{(1)}(t)}(l_j^{(1)^T}U)dx + l_j^{(1)^T}(A(x)U \\ - \nu_{j+\frac{1}{2}}^{(1)}U)|_{\tilde{x}_{j+\frac{1}{2}}^{(1)}(t)} - l_j^{(1)^T}(A(x)U - \nu_{j-\frac{1}{2}}^{(1)}U)|_{\tilde{x}_{j-\frac{1}{2}}^{(1)}(t)} \\ = \int_{\tilde{I}_j^{(1)}(t)} l_j^{(1)^T}F(x,t)dx.\end{aligned} \tag{A.4}$$

The first order ELDG discretization of Eq. (A.4) is to find $l_j^{(1)}U_h(x,t) \in P^0(\tilde{I}_j^{(1)}(t))$, so that

$$\begin{aligned}\frac{d}{dt}\int_{\tilde{I}_j^{(1)}(t)} l_j^{(1)^T}U_h dx = -\left[l_j^{(1)^T}\widehat{(A(x)U_h - \nu_{j+\frac{1}{2}}^{(1)}U_h)}|_{j+\frac{1}{2}}\right] \\ + \left[l_j^{(1)^T}\widehat{(A(x)U_h - \nu_{j-\frac{1}{2}}^{(1)}U_h)}|_{j-\frac{1}{2}}\right] \\ + \int_{\tilde{I}_j^{(1)}(t)} l_j^{(1)^T}F(x,t)dx \doteq L_1(U_h(t),t,\tilde{I}_j^{(1)}(t)).\end{aligned} \tag{A.5}$$

Here $\widehat{(A(x)U_h - \nu_{j+\frac{1}{2}}^{(1)}U_h)}$ at a cell boundary can be taken as a monotone flux, e.g. the Lax–Friedrichs flux

$$\begin{aligned}\widehat{(AU - \nu_{j+\frac{1}{2}}^{(1)}U)}_{j+\frac{1}{2}} = \frac{1}{2}\Big(A(x_{j+\frac{1}{2}}^+)U_{j+\frac{1}{2}}^+ - \nu_{j+\frac{1}{2}}^{(1)}U_{j+\frac{1}{2}}^+ + A(x_{j+\frac{1}{2}}^-)U_{j+\frac{1}{2}}^- \\ -\nu_{j+\frac{1}{2}}^{(1)}U_{j+\frac{1}{2}}^- - \alpha_{1,2}(U_{j+\frac{1}{2}}^+ - U_{j+\frac{1}{2}}^-)\Big)\end{aligned}$$

where $\alpha_{1,2} = max\{|\lambda^{(1)}(x_{j+\frac{1}{2}}) - \nu_{j+\frac{1}{2}}^{(1)}|, |\lambda^{(2)}(x_{j+\frac{1}{2}}) - \nu_{j+\frac{1}{2}}^{(2)}|\}$.

Similarly, we can easily update $l_j^{(2)^T}U_h$ related to $\lambda^{(2)}$ in the following:

$$\begin{aligned}\frac{d}{dt}\int_{\tilde{I}_j^{(2)}(t)} l_j^{(2)^T}U_h dx = -\left[l_j^{(2)^T}\widehat{(A(x)U_h - \nu_{j+\frac{1}{2}}^{(2)}U_h)}|_{j+\frac{1}{2}}\right] \\ + \left[l_j^{(2)^T}\widehat{(A(x)U_h - \nu_{j-\frac{1}{2}}^{(2)}U_h)}|_{j-\frac{1}{2}}\right] \\ + \int_{\tilde{I}_j^{(2)}(t)} l_j^{(2)^T}F(x,t)dx \doteq L_2(U_h(t),t,\tilde{I}_j^{(2)}(t)),\end{aligned} \tag{A.6}$$

where $l_j^{(2)^T}$ is a constant vector, locally defined on $\tilde{I}_j^{(2)}(t)$ approximating $l^{(2)^T}(x)$.

A simple first order ELDG scheme is composed by two evolution Eqs. (A.5) and (A.6). That is, we can update u_h^1 by (A.5), (A.6) and $u_h^1 = (r_j^{11} l_j^{(1)^T} + r_j^{12} l_j^{(2)^T}) U_h$:

$$\begin{aligned}\int_{I_j} u_h^{1,n+1} dx &= \int_{I_j} r_j^{11} l_j^{(1)^T} U_h^{n+1} dx + \int_{I_j} r_j^{12} l_j^{(2)^T} U_h^{n+1} dx \\ &= r_j^{11} \int_{I_j^{*,(1)}} l_j^{(1)^T} U_h^n dx + r_j^{11} \int_{t^n}^{t^{n+1}} L_1(U_h^{(1)}(t), t, \tilde{I}_j^{(1)}(t)) dt \\ &\quad + r_j^{12} \int_{I_j^{*,(2)}} l_j^{(2)^T} U_h^n dx + r_j^{12} \int_{t^n}^{t^{n+1}} L_2(U_h^{(2)}(t), t, \tilde{I}_j^{(2)}(t)) dt,\end{aligned} \tag{A.7}$$

where U_h^n and U_h^{n+1} are defined on the background mesh I_j, $U_h^{(1)}(t)$ and $U_h^{(2)}(t)$ are defined on the space–time dynamic meshes $\tilde{I}_j^{(1)}(t)$ and $\tilde{I}_j^{(2)}(t)$ respectively. Similarly, we can update u_h^2.

We apply forward-Euler method for time discretization with above ELDG scheme (A.7):

$$\begin{aligned}\int_{I_j} u^{1,n+1} dx &= r_j^{11} \int_{I_j^{*,(1)}} l_j^{(1)^T} U^n dx - \Delta t\, r_j^{11} l_j^{(1)^T} \\ &\quad \left[(A(x)\widehat{U^n - \nu}_{j+\frac{1}{2}}^{(1)} U^n)|_{x^{\star,(1)}_{j+\frac{1}{2}}} - (A(x)\widehat{U - \nu}_{j-\frac{1}{2}}^{(1)} U)|_{x^{\star,(1)}_{j-\frac{1}{2}}} \right] \\ &\quad + r_j^{12} \int_{I_j^{*,(2)}} l_j^{(2)^T} U^n dx - \Delta t\, r_j^{12} l_j^{(2)^T} \\ &\quad \left[(A(x)\widehat{U^n - \nu}_{j+\frac{1}{2}}^{(2)} U^n)|_{x^{\star,(2)}_{j+\frac{1}{2}}} - (A(x)\widehat{U - \nu}_{j-\frac{1}{2}}^{(2)} U)|_{x^{\star,(2)}_{j-\frac{1}{2}}} \right].\end{aligned} \tag{A.8}$$

Remark A.1 The above ELDG scheme is not conservative for two reasons:

(1) Flux terms can't cancel each other as $r_j^{11} l_j^{(1)^T}$ and $r_j^{12} l_j^{(2)^T}$ are discontinuous across cell boundary of $\Omega_j^{(1)}$, $\Omega_j^{(2)}$.

(2) $\sum_j r_j^{11} \int_{I_j^{*,(1)}} l_j^{(1)^T} U^n dx + r_j^{12} \int_{I_j^{*,(2)}} l_j^{(1)^T} U^n dx \neq \sum_j \int_{I_j} U^n dx$ because of the inconsistency in characteristic transformations between neighboring cells among $r_j^{11} l_j^{(1)^T}$ and $r_j^{12} l_j^{(2)^T}$.

B Appendix B: The Notation of Test Function

We give some notations which is used in the implementation of the fully discrete ELDG scheme with RK time discretization.

For convenience, we only give the definitions related to $\Omega_j^{(1)}$ below because we can similarly get the definitions related to $\Omega_j^{(2)}$. As scalar case, we take test function $\psi^{(1)}(x,t)$ as $\psi_{j,m}^{(1)}(x,t) = \Psi_{j,m}(x - \alpha^{(1)}(t - t^{n+1}))$ in the adjoint problem which is a set of basis of $P^k(\tilde{I}_j^{(1)}(t))$, where $\tilde{I}_j^{(1)}(t)$ is donated by a domain related $\lambda^{(1)}$ as $\tilde{I}_j(t)$ in scalar problem.

Here, we also take $\Psi_{j,m}$ as orthogonal basis on I_j, and let

$$u_h^{1,(1)}(x,t) = \sum_{l=0}^{k} \hat{u}_j^{1,(1);(l)}(t)\psi_{j,l}^{(1)}(x,t), \quad \text{on} \quad \tilde{I}_j^{(1)}(t), \tag{B.1}$$

where $\hat{u}^{1,(1);(l)}$ are coefficients for the basis. Let $\hat{U}_j^{1,(1)}(t) = (\hat{u}_j^{1,(1);(0)}(t), \ldots, \hat{u}_j^{1,(1);(k)}(t))^T$ be the coefficient vector of size $(k+1) \times 1$. Then we have

$$\left[\int_{\tilde{I}_j^{(1)}(t)} u_h^{1,(1)}(x,t)\psi_{j,0}^{(1)}(x,t)dx, \ldots, \int_{\tilde{I}_j^{(1)}(t)} u_h^{1,(1)}(x,t)\psi_{j,k}^{(1)}(x,t)dx\right]^T = \hat{U}_j^{1,(1)}(t), \forall t \in [t^n, t^{n+1}].$$

$\hat{U}_j^{2,(1)}(t)$ can be similarly defined.

Similar definition can be made to $\Omega_j^{(2)}$ and $\psi^{(2)}(x,t)$ for the second characteristics family.

References

1. Butler, D.S.: The numerical solution of hyperbolic systems of partial differential equations in three independent variables. Proc. R. Soc. Lond. Ser. A Math. Phys. Sci. **255**(1281), 232–252 (1960)
2. Cai, X., Guo, W., Qiu, J.-M.: A high order conservative semi-Lagrangian discontinuous Galerkin method for two-dimensional transport simulations. J. Sci. Comput. **73**(2–3), 514–542 (2017)
3. Cai, X., Qiu, J.-M., Yang, Y.: An Eulerian–Lagrangian discontinuous Galerkin method for transport problems and its application to nonlinear dynamics. J. Comput. Phys. **439**, 110392 (2021)
4. Celia, M., Russell, T., Herrera, I., Ewing, R.: An Eulerian–Lagrangian localized adjoint method for the advection–diffusion equation. Adv. Water Resour. **13**(4), 187–206 (1990)
5. Cockburn, B., Luskin, M., Shu, C.-W., Suli, E.: Enhanced accuracy by post-processing for finite element methods for hyperbolic equations. Math. Comput. **72**(242), 577–606 (2003)
6. Cockburn, B., Shu, C.-W.: TVB Runge–Kutta local projection discontinuous Galerkin finite element method for conservation laws. II. General framework. Math. Comput. **52**(186), 411–435 (1989)
7. Crouseilles, N., Mehrenberger, M., Vecil, F.: Discontinuous Galerkin semi-Lagrangian method for Vlasov–Poisson. In: ESAIM: Proceedings, vol. 32, pp. 211–230. EDP Sciences (2011)
8. Ding, M., Cai, X., Guo, W., Qiu, J.-M.: A semi-Lagrangian discontinuous Galerkin (DG)-local DG method for solving convection–diffusion equations. J. Comput. Phys. **409**, 109295 (2020)
9. Einkemmer, L., Ostermann, A.: Convergence analysis of a discontinuous Galerkin/Strang splitting approximation for the Vlasov–Poisson equations. SIAM J. Numer. Anal. **52**(2), 757–778 (2014)
10. Falk, R.S., Richter, G.R.: Explicit finite element methods for symmetric hyperbolic equations. SIAM J. Numer. Anal. **36**(3), 935–952 (1999)
11. Giraldo, F.X., Warburton, T.: A high-order triangular discontinuous Galerkin oceanic shallow water model. Int. J. Numer. Methods Fluids **56**(7), 899–925 (2008)
12. Guo, W., Nair, R., Qiu, J.-M.: A conservative semi-Lagrangian discontinuous Galerkin scheme on the cubed-sphere. Mon. Weather Rev. **142**(1), 457–475 (2013)
13. Hong, X., Xia, Y.: Arbitrary Lagrangian–Eulerian discontinuous Galerkin method for hyperbolic equations involving δ-singularities. SIAM J. Numer. Anal. **58**(1), 125–152 (2020)
14. Klingenberg, C., Schnücke, G., Xia, Y.: Arbitrary Lagrangian–Eulerian discontinuous Galerkin method for conservation laws: analysis and application in one dimension. Math. Comput. **86**(305), 1203–1232 (2017)
15. Kröger, T.: Multidimensional systems of hyperbolic conservation laws, numerical schemes, and characteristic theory: connections, differences, and numerical comparison. Ph.D. Thesis, Aachen, Techn. Hochsch., Diss., (2004)
16. Lax, P.: Systems of Conservation Laws. Technical report, LOS ALAMOS NATIONAL LAB NM (1959)
17. Lukáčová-Medvid'ová, M., Morton, K., Warnecke, G.: Evolution Galerkin methods for hyperbolic systems in two space dimensions. Math. Comput. **69**(232), 1355–1384 (2000)
18. Monk, P., Richter, G.R.: A discontinuous Galerkin method for linear symmetric hyperbolic systems in inhomogeneous media. J. Sci. Comput. **22**(1), 443–477 (2005)

19. Ostkamp, S.: Multidimensional characteristic Galerkin methods for hyperbolic systems. Math. Methods Appl. Sci. **20**(13), 1111–1125 (1997)
20. Qiu, J.-M., Shu, C.-W.: Positivity preserving semi-Lagrangian discontinuous Galerkin formulation: theoretical analysis and application to the Vlasov–Poisson system. J. Comput. Phys. **230**(23), 8386–8409 (2011)
21. Rossmanith, J.A., Seal, D.C.: A positivity-preserving high-order semi-Lagrangian discontinuous Galerkin scheme for the Vlasov–Poisson equations. J. Comput. Phys. **230**(16), 6203–6232 (2011)
22. Wang, K., Wang, H., Al-Lawatia, M.: An Eulerian–Lagrangian discontinuous Galerkin method for transient advection–diffusion equations. Numer. Methods Partial Differ. Equ. Int. J. **23**(6), 1343–1367 (2007)
23. Yoshida, H.: Construction of higher order symplectic integrators. Phys. Lett. A **150**(5–7), 262–268 (1990)
24. Zheng, N., Cai, X., Qiu, J.-M., Qiu, J.: A conservative semi-Lagrangian hybrid Hermite WENO scheme for linear transport equations and the nonlinear Vlasov–Poisson system. SIAM J. Sci. Comput. **43**(5), A3580–A3606 (2021)